Acta Pharmaceutica Sinica B 2024;14(8):3661−3679

Chinese Pharmaceutical Association
Institute of Materia Medica, Chinese Academy of Medical Sciences

Acta Pharmaceutica Sinica B

www.elsevier.com/locate/apsb
www.sciencedirect.com

ORIGINAL ARTICLE

Honey vesicle-like nanoparticles protect aged liver from non-alcoholic steatohepatitis

Baolong Liu[a,b,†], Phuong Linh Nguyen[a,c,†], Han Yu[a,c], Xingzhi Li[a], Huiren Wang[a], Tram Gia Bao Nguyen[a], Prakash Kumar Sahoo[a], Meghna Sur[d], Jay Reddy[d], Sarah Sillman[d], Stephen D. Kachman[e], Bara Altartouri[f], Guoqing Lu[g], Sathish Kumar Natarajan[a], Mahesh Pattabiraman[h], Jiujiu Yu[a,c,*]

[a]*Department of Nutrition and Health Sciences, University of Nebraska-Lincoln, Lincoln, NE 68583, USA*
[b]*Shaanxi Key Laboratory of Molecular Biology for Agriculture, College of Animal Science and Technology, Northwest A&F University, Yangling 712100, China*
[c]*Department of Nutrition, Case Western Reserve University, Cleveland, OH 44106, USA*
[d]*School of Veterinary Medicine and Biomedical Sciences, University of Nebraska-Lincoln, Lincoln, NE 68583, USA*
[e]*Department of Statistics, University of Nebraska-Lincoln, Lincoln, NE 68583, USA*
[f]*Center for Biotechnology, University of Nebraska-Lincoln, Lincoln, NE 68588, USA*
[g]*Department of Biology, University of Nebraska Omaha, Omaha, NE 68182, USA*
[h]*Department of Chemistry, University of Nebraska-Kearney, Kearney, NE 68849, USA*

Received 28 January 2024; received in revised form 23 April 2024; accepted 30 April 2024

KEY WORDS

Honey;
Extracellular vesicles;
Exosomes;
Nanoparticles;
microRNAs;
Aging;
Inflammation;
Non-alcoholic steatohepatitis

Abstract Non-alcoholic steatohepatitis (NASH), an advanced form of non-alcoholic fatty liver disease (NAFLD), has emerged as the leading cause of liver failure and related death. Currently, no medication is specifically approved to treat NAFLD or NASH. Here we report that oral administration of honey vesicle-like nanoparticles (H-VLNs) to naturally aged mice protects the liver from NASH development. H-VLNs are dominantly taken up by Kupffer cells in the liver and suppress hepatic chronic inflammation and further development of fibrosis and nodule formation in aged mice. Besides their reported anti-inflammasome function, H-VLNs are found to inhibit the transcriptional activities of C-JUN and nuclear factor-kappa B (NF-κB). MicroRNAs miR5119 and miR5108 and phenolic compound luteolin in H-VLNs are identified in suppressing both the C-JUN and NF-κB pathways. Collectively, oral intake of H-VLNs represents a promising new user-friendly modality to prevent the development of NASH.

*Corresponding author.
E-mail address: jxy1189@case.edu (Jiujiu Yu).
†These authors made equal contributions to this work.
Peer review under the responsibility of Chinese Pharmaceutical Association and Institute of Materia Medica, Chinese Academy of Medical Sciences.

https://doi.org/10.1016/j.apsb.2024.05.002
2211-3835 © 2024 The Authors. Published by Elsevier B.V. on behalf of Chinese Pharmaceutical Association and Institute of Materia Medica, Chinese Academy of Medical Sciences. This is an open access article under the CC BY-NC-ND license (http://creativecommons.org/licenses/by-nc-nd/4.0/).

© 2024 The Authors. Published by Elsevier B.V. on behalf of Chinese Pharmaceutical Association and Institute of Materia Medica, Chinese Academy of Medical Sciences. This is an open access article under the CC BY-NC-ND license (http://creativecommons.org/licenses/by-nc-nd/4.0/).

1. Introduction

Non-alcoholic fatty liver disease (NAFLD) is typified by excessive fat accumulation in the liver in humans who consume little or no alcohol[1]. The disease ranges from simple steatosis, characterized by ectopic accumulation of hepatic fat alone, to the more advanced form of non-alcoholic steatohepatitis (NASH) with clinical manifestations of steatosis, hepatocyte injury, and inflammation. NAFLD affects 30% of the general population worldwide and its prevalence in individuals over age 60 years has reached 40%[2,3]. The severity of NAFLD also increases with age, and its related complications often contribute to morbidity and mortality in the elderly population[2]. Currently, there is no specific licensed medication to treat NAFLD or NASH. In the early stages, lifestyle changes in diet and exercise are generally considered to be a first-line approach, but long-term adherence to these behaviors is low[4]. When the disease progresses to advanced NASH, the risk for the development of liver cirrhosis and hepatocellular carcinoma (HCC) is significantly increased. These life-threatening conditions often lead to liver failure, for which the sole treatment option is liver transplantation. Many patients with liver failure often face the fate of death because of the unavailability of healthy donor organs. Therefore, new approaches are urgently needed to protect the liver in general and especially in elderly NAFLD patients.

Honey, a sweet and flavorful liquid processed by bees from the nectar of flowers, has been used as a natural sweetener and traditional medicine since ancient times. Honey contains mainly sugars, which account for approximately 95%–97% of its dry weight, and a myriad of minor components such as vitamins, minerals, proteins, and phenolic compounds[5]. Recently, our group identified vesicle-like nanoparticles (VLNs) as a new component in honey[6]. Honey-derived VLNs (H-VLNs) are membrane-enclosed nanoparticles containing proteins, lipids, and small-sized RNAs. They potently inhibit activation of the nucleotide-binding domain and leucine-rich repeat related (NLR) family, pyrin domain containing 3 (NLRP3) inflammasome in primary macrophages. Intraperitoneal injection of H-VLNs ameliorates the level of circulating IL-1β, expression of inflammatory genes in the liver, and liver damage in lipopolysaccharide (LPS)/D-galactosamine-induced acute liver injury[6], in which the acute inflammation is mainly mediated by the NLRP3 inflammasome[7,8].

Although our initial study of H-VLNs[6] suggested that they possessed promising anti-inflammatory functions by targeting the NLRP3 inflammasome in an acute liver injury model, many questions remain unanswered. For example, it is not clear whether H-VLNs have any anti-inflammatory functions in the liver after oral intake. In addition, no studies have explored whether H-VLNs can ameliorate chronic inflammation in complex diseases like NASH. It would be important to investigate whether H-VLNs target any other inflammatory mediators besides the NLRP3 inflammasome. In the current study, we aimed to address these outstanding questions by orally administering H-VLNs to aged mice. Aging is an inevitable degenerative process that increases human/mouse susceptibility to many complex diseases, such as neurodegenerative diseases, NAFLD/NASH, and other metabolic diseases[9]. Along with aging comes chronic inflammation (sometimes termed inflammaging), which is a strong risk factor for the development of many aging-related diseases[9,10]. Aging-associated inflammation is complex; it involves NLRP3 inflammasome activation, as well as many other inflammatory mediators[11,12]. Thus, using aged mice would allow us to investigate the possible beneficial effects of H-VLNs on chronic inflammaging and the resulting aging-related diseases in multiple tissues, including NAFLD/NASH. We expected that our study would reveal the potential benefits of H-VLNs taken orally under chronic inflammation conditions and would improve our understanding of H-VLNs' new molecular targets and their responsible bioactive components. Most importantly, this study would promote the prospective oral intake of H-VLNs as a promising user-friendly hepatoprotective agent to curb NASH development.

2. Materials and methods

2.1. Cell culture

Bone marrow-derived macrophages (BMDMs) from C57BL/6J mice were cultured as described[7]. Huh7 hepatoma cells were grown in Dulbecco's modified Eagle's Medium (DMEM) with 4.5 g/L glucose (Corning, Tewksbury, MA, USA) containing 10% fetal bovine serum (FBS; Atlanta Biologicals, S11150, Minneapolis, MN, USA), 50 μg/mL PenStrep (Corning), and 2 mmol/L L-glutamine (Corning)[13]. Cell viability of BMDMs was determined using Cell Counting Kit-8 (Sigma, St. Louis, MO, USA) per the manufacturer's instructions. To assess the effects of H-VLNs or their biomolecules on C-JUN and nuclear factor-kappa B (NF-κB) pathways, BMDMs were incubated with H-VLNs for 16 h, and then treated with LPS (InvivoGen, tlrl-peklps, San Diego, CA, USA, 10 ng/mL) for 15 or 30 min. Cells were harvested for immunoblot analysis. To study the effects of H-VLNs or their biomolecules on target genes of C-JUN and NF-κB, BMDMs were incubated with H-VLNs for 16 h and then with LPS for 3 h. Cells were harvested for mRNA analysis.

Total H-VLN RNAs, each microRNA (miRNA) mimic (Qiagen, Germantown, MD, USA or ThermoFisher Scientific, Waltham, MA, USA) or AllStars negative control siRNA (Qiagen) were transfected in BMDMs using lipofectamine RNAiMAX (Invitrogen, Carlsbad, CA, USA) as described[6]. After 24 h transfection, LPS was incubated with BMDMs for 3 h, followed by mRNA analysis. Luteolin, syringic acid, vanillic acid, protocatechuic acid, and *p*-coumaric acid were purchased from Sigma, dissolved in ethanol, incubated with BMDMs for 16 h and then with LPS for 3 h. Afterward, cells were harvested for mRNA analysis.

2.2. Mice

C57BL/6J mice from Jackson Laboratory (Bar Harbor, ME, USA) were maintained in an animal facility free of specific pathogens

and fed with Teklad chow diet (Inotiv, 2016, West Lafayette, IN, USA). Animal experiments were approved by the Institutional Animal Care and Use Committee of the University (Project ID 2054). For the aging study, when 20 age-matched male mice reached 11.5 months old, they were randomly split into two groups (10 mice/group): the control group orally received phosphate-buffered saline (PBS) weekly and the treatment group orally received H-VLNs in PBS at 2×10^9/g. Their body weights were measured weekly. After seven months of treatment, the mice were subjected to a Barnes maze test. Each mouse was trained to locate the hiding hole on the maze table for six consecutive days and tested on Day 7. The time for each mouse to locate the hiding hole was recorded. The mice were rested for one week and re-tested on the maze table on Day 14. After eight months of treatment, the thigh bone density of each mouse was assessed using an UltraFocus DXA *in vivo* imaging system (BioVision, Milpitas, CA, USA). After 10.25 months, the mice were trained at 7 m/min for 10 min on a flat treadmill (Panlab, Holliston, MA, USA) for four consecutive days. On Day 5, the mice started to run at 6 m/min on a flat treadmill. Every 10 min, the run speed was increased 1 m/min. The mice were considered exhausted when they rested more than 30 consecutive seconds at the rear of the treadmill despite air puff stimulation (10−15 psi). After two more weeks of rest, the individual mice were subjected to metabolic cage analysis using a Phenomaster/Labmaster caging system (TSE Systems, Chesterfield, MO, USA). The mice were kept in the system for 48 h. The first 24 h was the adaptation period, and during the last 24 h period data were collected for analysis. When these mice reached 23 months old, they were sacrificed and their tissues were either snap-frozen with liquid nitrogen or fixed in 10% formalin solution (VWR, Radnor, PA, USA) for pathological, biochemical, and molecular analysis.

2.3. Extraction of H-VLNs and their biomolecules

Manuka honey (unprocessed, product of New Zealand, distributed by Wedderspoon, Malvern, PA, USA) was purchased from a local grocery shop, and H-VLNs were extracted as described[6]. Briefly, 2 g of honey was diluted with cold PBS, and the diluent was sequentially subjected to centrifugation at 500×*g* for 10 min and 2000×*g* for 20 min at 4 °C using an Allegra X-30 benchtop centrifuge (Beckman, Brea, CA, USA), followed by centrifugation at 10,000×*g* for 30 min at 4 °C using an Optima XE-90 ultracentrifuge (Beckman). The final supernatant underwent ultracentrifugation at 100,000×*g* for 2 h at 4 °C using the Optima XE-90 ultracentrifuge. The H-VLN pellets were washed with cold PBS, resuspended in PBS, and filtered using a 200 nm Acrodisc filter (Pall Laboratory, Port Washington, NY, USA). Alternatively, H-VLNs were subjected to further purification using the sucrose gradient (8%, 30%, and 60%)[6]. The size and yield of H-VLNs were measured by a NanoSight NS300 instrument (Malvern, Westborough, MA, USA)[14]. The protein concentration of H-VLNs was measured using the Micro BCA Protein Assay kit (ThermoFisher Scientific). Molecular composition analyses of H-VLNs were conducted as previously described[6]. To assess zeta potential, H-VLNs in PBS were diluted using double-distilled (dd) H_2O (1/100, *v*/*v*) to a final concentration of 0.5×10^{10}/mL (pH 7.4) and measured on a Litesizer 500 Particle Analyzer (Anton Paar, Vernon Hills, IL, USA). The measurement was repeated three times. After sucrose gradient ultracentrifugation, the high-purity H-VLNs were subjected to ultrastructure transmission electron microscopy (TEM) and conventional negative stain TEM as previously reported[6,15]. To disrupt the H-VLN structure, H-VLNs in PBS were sonicated using a digital sonifier S-450D (Branson, Brookfield, CT, USA) at 20% of maximal amplitude for a total of 2 min (20 s on and 10 s off), followed by bath sonication (Branson) 1 h at 37 °C. The samples were examined using a Hitachi HT7800 TEM at 80 kV, and micrographs were collected using an AMT NanoSprint1200 CMOS camera (Schaumburg, IL, USA).

RNAs were extracted from H-VLNs using miRNeasy Mini kit (Qiagen). To extract small chemicals from H-VLNs, four parts of a chloroform/methanol mixture (1/2, *v*/*v*) were mixed vigorously *via* vortex with one part of H-VLNs in PBS (1×10^{11} H-VLNs). 1.25 parts of chloroform and ddH_2O were sequentially added and mixed vigorously. The mixture was centrifuged at 1000×*g* for 10 min using an Allegra X-30 benchtop centrifuge (Beckman). The fraction soluble in chloroform (C-fraction) was collected, dried under nitrogen gas at 60 °C, and dissolved in 200 μL methanol. The leftover fractions soluble in water and methanol mixture (WM-fraction) were centrifuged at 10,000×*g* for 10 min. The supernatant was collected and dried under nitrogen gas at 60 °C until the volume reached 800 μL. 5 μL of the C-fraction, and 20 μL of the WM-fraction were incubated with BMDMs, followed by LPS treatment.

2.4. Identification of phenolic compounds in H-VLNs

The WM-fraction of H-VLNs was subjected to phenolic compound analysis using liquid chromatography-mass spectrometry (LC−MS) in the proteomics facility at the University of Nebraska Lincoln (UNL), following a previously reported procedure[16]. The high-performance liquid chromatography (HPLC) employed for the chromatographic separation was achieved with a Shimadzu Nexera ×2 system fitted with an Agilent Eclipse XDB C18 (100 mm × 3.0 mm; 3.5 μm particle size) reverse-phase column (Agilent, Santa Clara, CA, USA) maintained at ambient temperature; the HPLC system was coupled with a QTRAP 6500+ mass spectrometer (Sciex, Framingham, MA, USA) for tandem MS analysis. Mobile Phase: eluent A was a solution of 2% acetic acid in water and eluent B was 100% acetonitrile. Solvent gradient: 0−0.1 min, 6% B; 0.1−5 min, 6%−17% B; 5−8 min, 17%−20% B; 8−16 min, 90% B; 16−18 min, 90% B; 18−19 min, 6% at a flow rate of 0.4 mL/min. Sample injection volume is 1 μL.

The MS/MS system was operated with the IonDriveTM Turbo V electrospray ionization (ESI) source in positive and negative ion modes (Sciex). The ESI source operation parameters include: source temperature, 450 °C; ion spray voltage, 5500 and −4500 V; ion source gas 1, ion source gas 2, and curtain gas, 50, 50, and 25 psi, respectively; collision gas, medium. The MS/MS system was operated in multiple reaction monitoring (MRM) mode with optimized collision energy. The ionization voltages, MRM transition ions (precursor and product ions), collision energy, declustering potential, entrance potential, and collision cell exit potential were optimized by a Sciex Analyst software package[16]. Analytical data were processed using the Analyst 1.6.3 software platform (Sciex). Chemicals were identified based on retention time matching with standards purchased from Sigma and their MS/MS profiles. Retention time matching and ESI-MS of signals were performed on a single quad Agilent 1260 infinity LC−MS.

2.5. Labeling and uptake of H-VLNs

To study the distribution of H-VLNs in mice, H-VLNs were covalently labeled with a fluorescent dye from an ExoGlow-Vivo EV labeling kit (System Biosciences, EXOGV900A-1, Palo Alto,

CA, USA) and orally administered to 2-year-old male C57BL/6J mice at 60,000 fluorescence intensity/g. Six hours later, the mice were sacrificed to collect a variety of organs. The fluorescence signals of organs were assessed using an Odyssey Clx imaging platform (LI-COR Biosciences, Lincoln, NE, USA). The dose and waiting time were determined based on the pilot experiments, as well as our previous study showing that 60,000 fluorescence intensity/g of garlic chive-derived VLNs was needed to detect fluorescent signals in other organs besides the gastrointestinal (GI) tract[7].

To identify the target cell types in the liver, H-VLNs were labeled with PKH26 (Sigma) per the manufacturer's manual and given *via* intravenous injection to 2-year-old male C57BL/6J mice at 600 fluorescence intensity/g daily for three days. On Day 4, the mice were sacrificed, and the livers were frozen in Tissue-Tek O.C.T. Compound (Sakura Finetek, Torrance, CA, USA) for further immunohistofluorescence (IHF) staining. For the cell culture experiment, H-VLNs were labeled with PKH26 and incubated with either BMDMs or Huh7 cells for 16 h. Cells were washed with PBS three times, fixed using 4% paraformaldehyde (Sigma), and their images taken using an A1R−Ti2 confocal fluorescence microscope (Nikon, Melville, NY, USA).

2.6. Pathological analysis of tissue samples

The fixed liver samples were embedded in paraffin, sliced into 4 μm thick sections, subjected to routine hematoxylin and eosin (H&E) staining in the UNL Veterinary Diagnostic Laboratory, and their images taken using an EVOS™ M7000 imaging system (Invitrogen). The following parameters scored with modifications as per Liang et al[17] as an adapted rodent model grading system for NAFLD: inflammatory cell infiltration score (grades 0−3), macrovesicular steatosis score (grades 0−3), hepatocellular hypertrophy score (grades 0−3), and microvesicular steatosis score (grades 0−3). According to this system, an inflammatory focus was defined as a grouping of at least five inflammatory cells clustered together and not arranged in a row; these were quantified using five 100 × magnification (field of view 3.1 mm^2) fields by averaging the number per 100 × field. To attempt representation of samples with more extensive inflammatory cell infiltrates, the foci of inflammation measuring greater than 100 μm in the hepatic lobules were counted in five 100 × fields, averaged, and termed "lobular inflammatory foci." For inflammation, grades were reported as the average number of inflammatory foci per field. Grade 0: <0.5; grade 1: 0.5−1; grade 2: 1−2; grade 3: >2. Macrovesicular steatosis was defined as the presence of one or a few large cytoplasmic lipid vacuoles that displaced the nucleus to the side; microvesicular steatosis was defined as the presence of small lipid vacuoles that did not significantly displace the nucleus peripherally. Total hepatocellular steatosis was the sum of both macrovesicular and microvesicular steatosis. Hepatocellular hypertrophy was defined only as abnormal enlargement of the cell (at least 1.5 times the diameter of expected normal size) regardless of nuclear enlargement or cytoplasmic changes like vacuolation. These parameters were evaluated across the entire histologic section, varying from 100 × to 200 × field views to examine the morphology of the cells. Grade 0: <5% of the hepatic parenchyma; grade 1: 5%−33%; grade 2: 33%−66%; and grade 3: >66%.

2.7. Sirius red staining

The liver sections were heated at 56 °C for 45 min and washed in xylene substitute (Electron Microscopy Sciences, 23412−01, Hatfield, PA, USA) 3 times to remove paraffin. The tissues were rehydrated by sequentially immersing the slides in decreasing concentrations of ethanol (100%, 95%, 70%, 50%, and 30%) for 5 min each, stained with picro-sirius red solution (0.1% Sirius red in saturated picric acid solution) for 1 h, and washed 5 times in acidified water (0.5% acetic acid in ddH_2O) for 5 min. After removing the water, the slides were dehydrated in 100% ethanol (5 min, 3 times). The tissues were scored for hepatic fibrosis (stages 0−4) as defined by Kleiner et al[18]. Small amounts of collagen around vessels were considered normal. Fibrosis extent was determined after examination of the entire section at 100 to 200 × magnification. Stage 0: none; stage 1: mild or moderate, perisinusoidal or periportal fibrosis; stage 2: perisinusoidal and periportal fibrosis; stage 3: bridging fibrosis; stage 4: cirrhosis.

2.8. Immunohistochemistry (IHC) staining

The liver sections were dewaxed as described for Sirius red staining. The sections were incubated in 100% ethanol (10 min, 2 times), 95% ethanol (10 min, 2 times), and ddH_2O (5 min, 2 times) for tissue rehydration. Antigen retrieval was followed by immersing the sections in sub-boiling (95−98 °C) citrate solution (10 mmol/L sodium citrate, 0.05% Tween-20, pH 6.0) for 10 min. After the sections were cooled to room temperature, they were washed in ddH_2O (5 min, 2 times). The tissue samples were incubated with 3% H_2O_2 (10 min), washed with ddH_2O (5 min, 2 times) and Tris-buffered saline with 0.1% Tween-20 (TBST, 5 min), blocked with 5% bovine serum albumin (BSA) in PBS (1 h), and incubated with primary antibody overnight at 4 °C. Next day, the tissue samples were rinsed in TBST, incubated with horseradish peroxidase (HRP)-conjugated anti-rabbit secondary antibody SignalStain Boost IHC detection reagent (Cell Signaling, Danvers, MA, USA) for 30 min, washed with TBST (5 min, 3 times), developed using SignalStain DAB substrate kit (Cell signaling) for 10−30 min, and washed with ddH_2O (5 min). The nucleus counterstain was achieved by incubating tissue samples with hematoxylin solution (5 min, Sigma) and washing with ddH_2O (5 min, 2 times). The sections were incubated in 95% ethanol (10 s, 2 times), 100% ethanol (10 s, 2 times), and xylene (10 s, 2 times) for dehydration. The slides were mounted using DPX Mountant (ThermoFisher Scientific). Primary antibodies used included antibodies against SRC (Cell Signaling, Cat. No. 2109, dilution, 1/3000, *v/v*), F4/80 (Cell Signaling, Cat. No. 70076, dilution, 1/200, *v/v*), α-smooth muscle actin (α-SMA, Cell Signaling, Cat. No. 19245, dilution, 1/400, *v/v*), KI67 (Cell Signaling, Cat. No. 12202, dilution, 1/200, *v/v*), and P65 (Cell Signaling, Cat. No. 8242, dilution, 1/400, *v/v*).

2.9. IHF, immunofluorescence (IF), and terminal deoxynucleotidyl transferase dUTP nick end labeling (TUNEL) staining

Liver tissues frozen in O.C.T. Compounds were used for IHF staining. The sections from cryosection were fixed in 4% paraformaldehyde on ice for 8 min and washed with PBS (5 min, 3

times). The tissue samples were blocked with 2% BSA in PBS for 30 min and incubated with primary antibodies overnight at 4 °C. Next day, the samples were rinsed with PBS 3 times, incubated with a secondary antibody for 30 min at room temperature, and washed with PBS 3 times. The dried slides were mounted using ProLong Gold Antifade Mountant with SYTOX deep red (ThermoFisher Scientific). Primary antibodies were antibodies against F4/80-Alexa Fluor 488 (BioLegend, Cat. No. 123119, San Diego, CA, USA, dilution, 1/100, *v/v*), KERATIN 18 (ProteinTech Group, Cat. No. 10830-1-AP, Rosemont, IL, USA, dilution, 1/200, *v/v*), DESMIN (Cell Signaling, Cat. No. 5332, dilution, 1/100, *v/v*), CD146-APC (Milenyi Biotech, Cat. No. 130-102-846, Auburn, CA, USA, dilution, 1/20, *v/v*), and ASC (Adipogen, Cat. No. AG25B0006C100, San Diego, CA, USA, dilution, 1/200, *v/v*). IF staining of macrophages was performed as previously described[19]. Primary antibodies used were anti-P65 (Cell Signaling, Cat. No. 8242, dilution, 1/400, *v/v*) and anti-phospho-C-JUN (Cell Signaling, Cat. No. 3270, dilution, 1/800, *v/v*). TUNEL staining of liver sections was conducted as described[20].

2.10. Immunoblot and mRNA analysis

Immunoblot and mRNA analysis were carried out as described[6]. Primary antibodies used in this study were antibodies recognizing inhibitor units of κB (IκBα, Cell Signaling, Cat. No. 4841, dilution, 1/1000, *v/v*), phospho-JUN N-terminal kinases (JNK, Cell Signaling, Cat. No. 4668, dilution, 1/1000, *v/v*), JNK (Cell Signaling, Cat. No. 9252, dilution, 1/1000, *v/v*), phospho-C-JUN (Cell Signaling, Cat. No. 3270, dilution, 1/1000, *v/v*), C-JUN (Cell Signaling, Cat. No. 9165, dilution, 1/1000, *v/v*), NLRP3 (Adipogen, Cat. No. AG20B0014C100, dilution, 1/1000, *v/v*), ASC (Adipogen, Cat. No. AG25B0006C100, dilution, 1/1000, *v/v*), CASP1 P10 (Adipogen, Cat. No. AG20B0044C100, dilution, 1/1000, *v/v*), IL-1β (R&D systems, Cat. No. AF401NA, Minneapolis, MN, USA, dilution, 1/2000, *v/v*), and TUBULIN (Santa Cruz, Cat. No. SC-5286, Dallas, TX, USA, dilution, 1/200, *v/v*).

2.11. Measurement of plasma liver injury markers and liver triacylglycerol

The levels of liver injury markers alanine aminotransferase (ALT) and aspartate aminotransferase (AST) in plasma were measured using a Vitros-250 Chemistry Analyzer (Johnson & Johnson, New Brunswick, NJ, USA). The levels of hepatic triacylglycerol were measured using a TG colorimetric assay kit (Cayman Chemicals, Ann Arbor, MI, USA).

2.12. RNA extraction and sequencing

Total mRNA was extracted from liver samples using an RNeasy extract kit (Qiagen) following the manufacturer's instructions. RNA integrity and quantity were assessed using a 2200 TapeStation system (Agilent). The RNA samples were subjected to sequencing. Specifically, a total of 1 μg RNA with an RNA integrity number >7 was used for RNA-Seq library construction. A cDNA library was constructed using the TruSeq Stranded mRNA LT Sample Prep Kit-Set A (Illumina, San Diego, CA, USA), amplified using PCR, and sequenced using the Illumina NextSeq sequencing system with a Hi-Output (75 cycles) sequencing kit.

2.13. Transcriptomic data processing and analysis

Raw reads were quality-checked using FastQC[21] and processed by trimming the first 14 bases and the last two bases using the Trim Sequences program[22]. Cleaned reads, approximately 40 million reads/sample, were mapped to the mouse (*Mus Musculus*) reference genome, mm10 Full, with HISAT2[23]. The mapped files were used to assess gene expression, *i.e.*, the number of reads mapped to a given transcript using featureCounts[24]. DESeq2 was used to identify differentially expressed genes in H-VLN-treated *versus* PBS control samples or in aged livers *versus* young healthy livers[25]. Genes with an adjusted *P*-value <0.05 were considered significant and were used to generate the volcano plots using imageGP[26]. Gene set enrichment analysis (GSEA)[27] software was utilized to analyze the enrichment of specific gene sets in aged livers (compared to young livers) or in H-VLN-treated mice (compared to control aged mice). The top 50 upregulated genes with *P*-value <0.05 from gene expression data (NCBI GEO database GSE135050) were selected to create the two reference steatosis gene sets. For the H-VLN-treated group, differentially expressed genes (compared to control aged mice) with the cut-off criterion of absolute fold-change >1.5 and *P*-value <0.05 were selected for further bioinformatics analysis. The Metascape online database (https://metascape.org)[28] was used to analyze gene ontology biological processes, the Kyoto encyclopedia of genes and genomes (KEGG) pathway, Reactome gene sets, WikiPathways, and transcriptional regulatory relationships unraveled by sentence-based text (TRRUST) mining. Protein−protein interaction (PPI) network analysis was carried out using the STRING, BioGrid, and OmniPath database from Metascape, followed by Molecular Complex Detection (MCODE) analysis to identify densely connected network components within the PPI.

2.14. Statistics

The data from cell culture experiments were analyzed using Excel software. A two-tailed *t*-test was used to compare the differences between the two conditions. Each cell culture experiment was repeated 3−4 times. R version 3.6.0 (R Core Team, The R Foundation for Statistical Computing, Vienna, Austria)[29] was employed to analyze the data from animal experiments. The normality of the data was first assessed using a Shapiro−Wilks test. A low *P*-value from this test suggested that the data were not normally distributed. In this case, the data were further analyzed using a nonparametric Mann−Whitney test. Otherwise, the data were considered to be normally distributed and analyzed using a two-tailed *t*-test. The results were considered significant when $P < 0.05$ (n.s., $P > 0.05$; $^{*}P < 0.05$; and $^{**}P < 0.01$).

3. Results

3.1. Characterization of H-VLNs and their in vivo distribution in aged mice

H-VLNs were extracted from monofloral manuka honey using the ultracentrifugation method[6], and visualized by negative stain TEM, one of the most widely used methods for extracellular vesicle (EV) or VLN imaging[30]. H-VLNs generally showed spherical morphology, with sizes of 50−100 nm in diameter (Fig. 1A). Ultrastructure TEM at high magnification revealed the

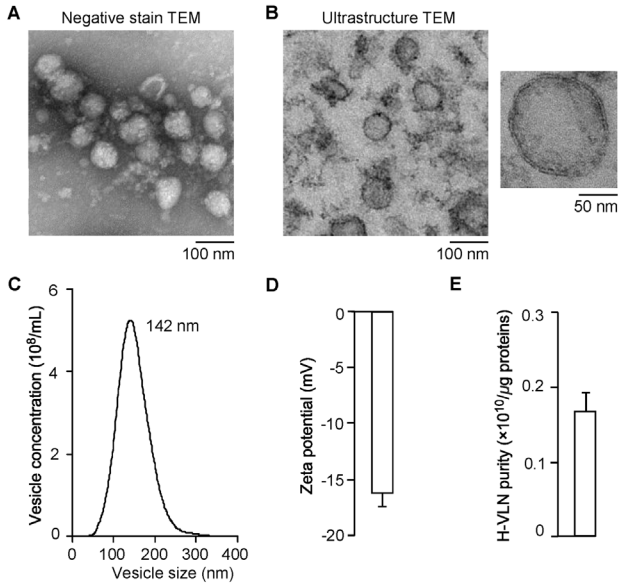

Figure 1 Characterization of H-VLNs. (A) Representative negative stain TEM image of H-VLNs. (B) Representative ultrastructure TEM image of H-VLNs. (C) Size distribution of H-VLNs measured using a NanoSight NS300 instrument. (D) Zeta potential of H-VLNs. H-VLNs in PBS were diluted using ddH_2O (1/100, *v*/*v*) to a final concentration of 0.5 × 10^{10}/mL (pH 7.4) and measured on a Litesizer 500 Particle Analyzer. Data were presented as mean ± SEM (n = 3). (E) Purity of H-VLNs. The H-VLN purity was determined by comparing the ratio of nanoparticle counts to protein concentration. Data presented as mean ± SEM (n = 4). Scale bar = 50 or 100 nm.

bilayer membrane-enclosed vesicle-like structure of H-VLNs (Fig. 1B). Nanoparticle tracking analysis indicated that H-VLNs, on average, measured 142 nm in diameter (Fig. 1C). The zeta potential of H-VLNs was −16.3 ± 0.3 mV (Fig. 1D). H-VLN purity was assessed by comparing the ratio of nanoparticle counts to protein concentration[31]. The ratio of H-VLNs was 0.17 ± 0.03 × 10^{10}/μg (Fig. 1E), comparable to that of EVs from the culture media of cancer cell lines[31]. Consistent with our previous findings[6], the yield of H-VLNs from manuka honey was approximately 7−8 × 10^{10}/g; they contained small-sized RNAs and a series of proteins and lipids (Supporting Information Fig. S1A−S1C). The RNA and protein profiles of H-VLNs were reported in detail in our previous study[6]. The lipid profile of H-VLNs was not successfully characterized.

A fluorescent dye from an ExoGlow-Vivo EV labeling kit was used to covalently label the membrane proteins of H-VLNs, and such labeled H-VLNs were orally administered to aged mice. This covalent labeling approach ensured a stable attachment of the fluorescent dye to H-VLNs after oral administration and excluded possible dye dissociation or release, which were often observed with the lipophilic fluorescent dyes[32]. Interestingly, fluorescent signals were detected mainly in the GI tract and liver (Supporting Information Fig. S2A and S2B), indicating that H-VLNs could be absorbed through the GI tract and accumulate in the liver. The fluorescent signals of H-VLNs in livers accounted for 2.1 ± 0.9% of total fluorescent signals in all tissues.

3.2. *Physiological characterization of aged mice treated with H-VLNs*

Age-matched male C57BL/6J mice were maintained in a specific pathogen-free animal facility and fed with a chow diet during the entire experiment. When they reached 11.5 months of age, they were orally administered the solvent PBS or H-VLNs in PBS each week for 11.5 months (Fig. 2A). The body weights of the mice in the PBS control group and the H-VLN-treated group were similar (Supporting Information Fig. S3A). After 7 months of H-VLN treatment, the mice were subjected to a Barnes maze test; the two groups took a similar amount of time to locate the hiding hole on the maze table in the initial test (Supporting Information Fig. S3B). However, after one week of rest, the mice from the H-VLN-treated group generally located the hiding hole more quickly, although the time difference did not reach statistical significance (Supporting Information Fig. S3B), suggesting that H-VLNs may have the potential to improve cognitive function during aging. It would be interesting to investigate the possible benefits of H-VLNs in preventing cognitive declination due to aging, Alzheimer's disease, or other dementia conditions in the future.

No significant difference was observed in thigh-bone density between the control and treatment groups (Supporting Information Fig. S3C). After the mice were treated with H-VLNs for 10.25 months, the average run distances of the two groups were comparable in an endurance run test (Supporting Information Fig. S3D). Two weeks later, the mice were subjected to metabolic cage analysis. Heat production, oxygen consumption rate, CO_2 production rate, respiratory exchange ratio, food intake, and water intake were similar in the two groups (Supporting Information Fig. S3E−S3H). The H-VLN-treated mice tended to move more frequently and be more active during the night than the control mice (Supporting Information Fig. S3I), implying that the H-VLN-treated mice may have had a higher level of energy that made them more willing to move.

3.3. *H-VLNs protected the liver from NASH in aged mice*

After 11.5 months of H-VLN treatment, the mice reached 23 months of age and were sacrificed. During the sacrifice, two mice in the control group showed macroscopically visible hepatic fibrosis and three had one or more liver nodules (one mouse showed both fibrosis and nodules); however, none of the mice in the H-VLN-treated group showed any macroscopically visible fibrosis or nodules in the liver (Fig. 2B). The ratio of liver to body weight was comparable in the two groups (Fig. 2C). The levels of circulating ALT, a commonly used liver injury marker[33], tended to be lower in the H-VLN-treated mice, but the decrease did not reach statistical significance (Fig. 2D). The levels of circulating AST were similar in the two groups (Fig. 2E).

Liver sections from all the mice were subjected to H&E staining. Remarkably, livers from aged mice in the control group generally showed steatosis and immune cell infiltration (Fig. 2F, left panel), which were typically observed in a variety of diet-induced NASH mouse models[34]. To assess the NASH severity and penetration in these aged mice, H&E-stained liver sections were evaluated semi-quantitatively using a modified NAFLD

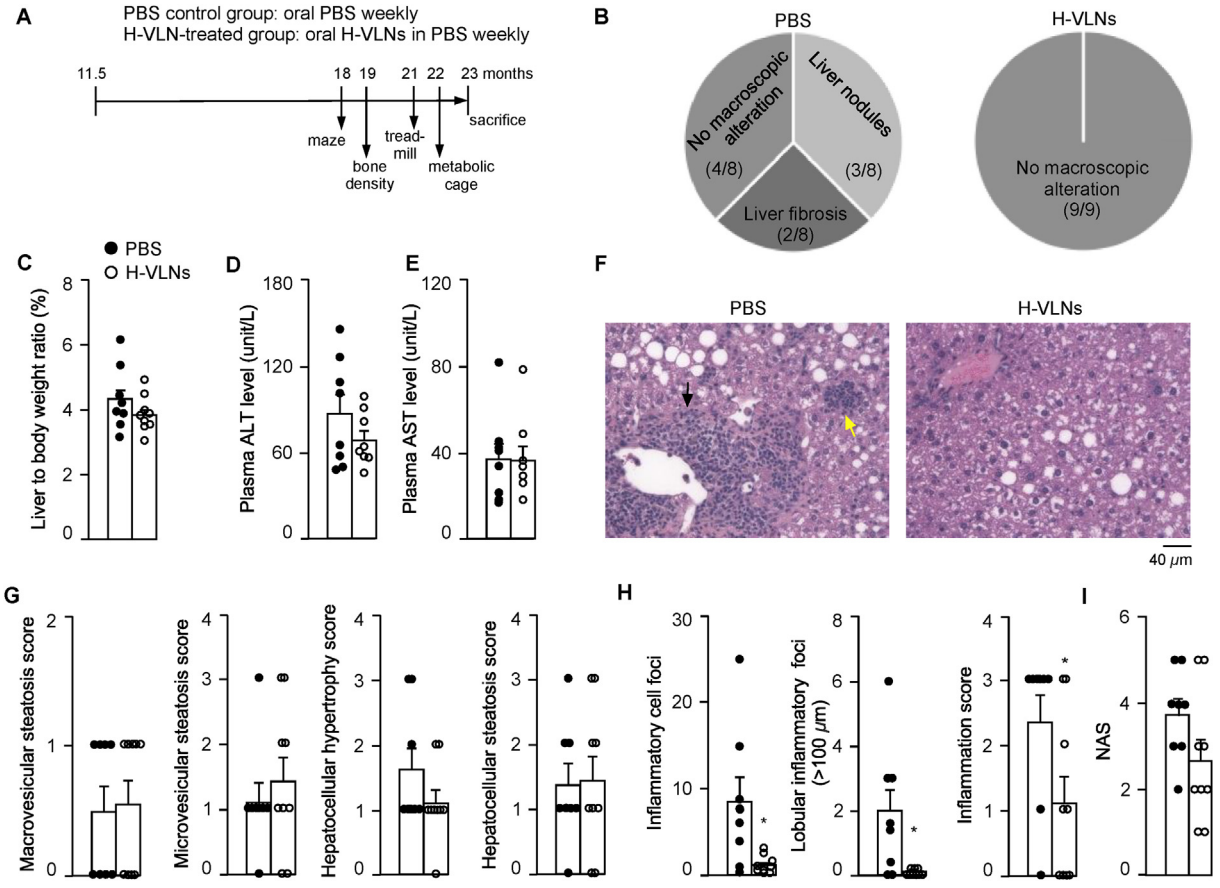

Figure 2 H-VLNs protected liver from NASH in aged mice. (A) Schematic diagram showing the experimental procedure. 11.5-month-old male C57BL/6J mice received either the solvent PBS (PBS control group) or 2×10^9/g H-VLNs in PBS (H-VLN-treated group) each week through oral gavage ($n = 10$/group). The mice were subjected to a series of physiological tests and sacrificed at the age of 23 months. Maze: Barnes maze test. One or two mice died in each group by the end of the study due to aging. (B) A summary of macroscopic alteration in the liver. (C) Ratio of the liver to body weight. (D) Plasma ALT level. (E) Plasma AST level. (F) Representative images of H&E staining of liver sections showed massive immune cell infiltration in the livers of control mice but not in those of H-VLN-treated mice. The black arrow indicates the perivascular inflammatory foci and the yellow arrow indicates the lobular inflammatory foci in the control liver. (G) Scores of macrovesicular steatosis, microvesicular steatosis, hepatocellular hypertrophy, and overall hepatocellular steatosis of mouse livers. (H) Inflammatory cell foci, large lobular inflammatory foci (>100 μm), and inflammation score of livers. In G and H, each mouse was graded from 0 to 3 (grading details were described in Materials and methods) and indicated as one dot in the bar graphs. (I) NAS of both groups. NAS was the unweighted sum of steatosis, inflammation, and ballooning scores. Ballooning scores were zero in both groups. In G to I, when multiple mice were ranked in the same grade or had the same focus number, their dots were spread out horizontally. $n = 8$ to 9/group. Data were presented as mean ± SEM. *$P < 0.05$ and **$P < 0.01$ *vs.* indicated (bar with black dots). Scale bar = 40 μm.

scoring system for rodent models in a blinded manner[17]. Consistent with the steatosis features found in diet-induced NAFLD mouse models[17], livers from our aged mice manifested macrovesicular steatosis, microvesicular steatosis, and hepatocellular hypertrophy (Fig. 2F and G). The scores of each type of steatosis and overall steatosis were comparable between control and H-VLN-treated groups (Fig. 2G). In support of the histological analysis, quantitative measurement of hepatic triacylglycerol content (Supporting Information Fig. S4A) and expression levels of lipogenic *Srebf1* and *Fasn* genes (Supporting Information Fig. S4B) in the two groups confirmed that H-VLNs did not affect steatosis at the biochemical and molecular levels. Blinded histological assessment of H&E-stained liver sections showed high percentages of inflammatory cell foci in the aged livers of the control group (Fig. 2F and H). The inflammation score of aged mice in the control group was 2.4 ± 0.4 (Fig. 2H), which was higher than that (1.5 ± 0.5) found in C57BL/6J mice fed with a high-fat, -cholesterol, and -fructose (HFCF) diet for seven months[35]. Interestingly, the inflammation was largely curbed in the H-VLN-treated groups (Fig. 2F and H). Of note, we found that the aged mice in both groups lacked hepatocyte ballooning (an important histologic marker of human NASH[36]), in agreement with multiple diet-induced NASH mouse models[17]. Finally, a NAFLD activity score (NAS), which was the unweighted sum of steatosis, inflammation, and ballooning scores[18], was calculated for both groups. The NAS of aged mice in the control group was 3.8 ± 0.4, which was comparable to the NAS levels (ranging from 3 to 5) of NASH mouse models induced by feeding with a high-fat, -cholesterol, and -fructose/sucrose diet for 3−6 months[35,37,38]. This NAS was alleviated in H-VLN-treated mice, but the difference did not reach statistical significance (Fig. 2I).

Together, the pathohistological assessments suggested that our aged mice spontaneously developed NASH, as well as macroscopically visible fibrosis and nodules. H-VLNs had no impact on

steatosis but did protect aged livers from inflammation, visible fibrosis, and nodule formation.

mRNAs from the livers of control and H-VLN-treated aged mice, as well as mRNAs from the livers of five 12-week-old male C57BL/6J mice fed with a chow diet, were subjected to RNA-seq analysis. First, the aged mice in the control group were compared to the young healthy mice to further evaluate the NASH condition in aged mice at the molecular level. The volcano plot showed that many genes were markedly up- or down-regulated in aged livers, compared to young livers (Supporting Information Fig. S5A). The gene expression profile of aged mice *versus* young mice was subjected to GSEA[27] for phenotype interpretation. Using the existing gene sets (mouse collections) from the Molecular Signature Database (MsigDB), we found that upregulated genes in aged mice were highly related to inflammation (MsigDB ID: MM3890), fibrosis (MM12425), and HCC (MM535, Fig. S5B−S5D). The gene set "collagen-containing extracellular matrix" (MM12425) was used as the indicator of fibrosis because the fibrous scar results from the accumulation of extracellular matrix proteins (mostly crosslinked collagens). The gene set "liver cancer" (MM535) was based on the genes that were highly over-expressed in liver tumors in *Txnip*$^{-/-}$ mice, compared to non-tumor hepatic tissues[39]. MsigDB does not have an existing reference gene set for steatosis. Recently, in a time course study[35] of a NAFLD mouse model induced by an HFCF diet, an RNA-seq analysis was conducted on hepatic mRNAs from chow-fed and HFCF-fed male C57BL/6J mice at 1-month and 3-month time points. The mice fed with an HFCF diet for one month began to show steatosis in the livers, which became more prevalent in the mice fed with the HFCF diet for three months. We used the dataset from this study (NCBI GEO database GSE135050) to create new reference gene sets named "1-month diet-induced steatosis" and "3-month diet-induced steatosis." The gene expression profiles of our aged mice *versus* young mice began to show a positive correlation with "1-month diet-induced steatosis" and significantly correlated with "3-month diet-induced steatosis" (Fig. S5E). Therefore, the hepatic transcriptome data indicated that the aged livers underwent comprehensive transcriptional activation of genes related to steatosis, inflammation, fibrosis, and HCC.

Notably, compared to control aged livers, many genes were down-regulated in the livers of H-VLN-treated mice, as shown by the volcano plot (Supporting Information Fig. S6A). GSEA indicated that H-VLN treatment was significantly inverse-correlated with inflammatory response, fibrosis, and HCC (Fig. 3A). Further ingenuity pathway analysis (IPA) demonstrated that most of the H-VLN-regulated genes were related to hyperplasia, inflammation, fibrosis, HCC, and liver damage (Fig. 3B). Metascape analysis was used to visualize the PPI networks of H-VLN-suppressed genes, and 17 network components were identified by the MCODE algorithm (Fig. 3C and Fig. S6B), many of which belonged to inflammatory response, fibrosis, and HCC. Thus, H-VLN treatment seemed to curb, at least to a certain extent, the NASH-favored transcriptional rewiring in aged mice.

3.4. *H-VLNs inhibited hepatic inflammation in aged mice*

Of note, the inflammasome pathway in the liver was significantly suppressed by H-VLNs (Fig. 3C), which was consistent with our previous report that H-VLNs potently inhibited NLRP3 inflammasome activity[6]. The NLRP3 inflammasome is composed of three subunits: the sensor NLRP3, the adaptor apoptotic speck protein containing a caspase recruitment domain (ASC), and the effector CASPASE-1 (CASP1)[40]. In response to danger or stress stimuli from pathogens, the environment, or the host, the NLRP3 inflammasome subunits are assembled into an active protein complex, in which the active CASP1 cleaves pro-interleukin (IL)-1β to release mature IL-1β. This potent cytokine mediates many downstream inflammatory responses. Inappropriate activation of the NLRP3 inflammasome triggers and/or maintains chronic inflammation in NAFLD, obesity, and many other complex diseases[40,41]. mRNA analysis showed that transcription of the *Nlrp3, Pycard (Asc), and Casp1* genes in the liver was significantly suppressed in H-VLN-treated mice (Fig. 4A). At the protein level, both NLRP3 and CASP1 were reduced in H-VLN-treated livers, but ASC remained at similar levels in the two groups (Fig. 4B). H-VLNs tended to suppress transcription of the *Il1b* gene in the liver (Fig. 4A) and dramatically decreased the hepatic protein level of pro-IL-1β (Fig. 4B). We were not able to detect the mature cleaved IL-1β in hepatic lysates, likely due to its low level. Upon inflammasome activation, inflammasome subunits (NLRP3, ASC, and CASP1) oligomerize and form a high-molecular-mass multi-protein complex. This active inflammasome complex can be visualized under confocal microscopy as a single ASC speck in each cell using an anti-ASC antibody[6,42]. Through ASC IHF staining, ASC specks (*i.e.,* the active inflammasome complex) were readily detected in aged livers (Fig. 4D, left panel). Notably, quantification of ASC specks (Fig. 4C) showed that H-VLN treatment significantly reduced the number of ASC specks in the liver sections, suggesting that H-VLNs effectively reduced active inflammasome formation in the liver. IHC staining using an antibody against F4/80 (a macrophage marker[43]) showed massive infiltration of macrophages/Kupffer cells in the livers of control mice, but such infiltration was largely curbed by H-VLN treatment (Fig. 4E and F). mRNA levels of a number of pro-inflammatory genes, such as *Adgre1, Il6, Tnf, Ccr2, Tlr4, Ccl3,* and *Cxcl5*, were significantly decreased in the livers of H-VLN-treated mice compared to those of control mice (Fig. 4G). In contrast, the expression of anti-inflammatory genes, including *Il10* and *Il13*, were prominently augmented in the H-VLN-treated group, compared to the control mice (Fig. 4H). Taken together, these data suggested that H-VLNs suppressed hepatic inflammation in aged mice.

3.5. *H-VLNs inhibited the development of fibrosis and hepatocarcinogenesis in aged mice*

Chronic inflammation in the liver leads to fibrosis and eventually cirrhosis[44]. The persistently active inflammatory cells and their released cytokines and chemokines activate hepatic stellate cells (HSCs), which secrete extracellular matrix proteins that form the fibrous scar. Because of alleviated hepatic inflammation (Fig. 4) and the absence of macroscopically visible hepatic fibrosis in H-VLN-treated mice (Fig. 2B), we further assessed fibrosis at the histopathological and molecular levels. Sirius red collagen staining demonstrated severe liver fibrosis and abnormal liver architecture in control mice (Fig. 5A, left panel), but was not observed in H-VLN-treated aged mice (Fig. 5A, right panel). These Sirius red-stained liver sections were subjected to blinded grading of fibrosis as defined by the NASH Clinical Research Network[18]. The hepatic fibrosis scores of control and H-VLN-treated aged mice were 2 ± 0.27 and 1.1 ± 0.26, respectively (Fig. 5C), indicating that hepatic fibrosis was markedly attenuated in the H-VLN-treated mice. α-SMA is a proven valuable marker for activated

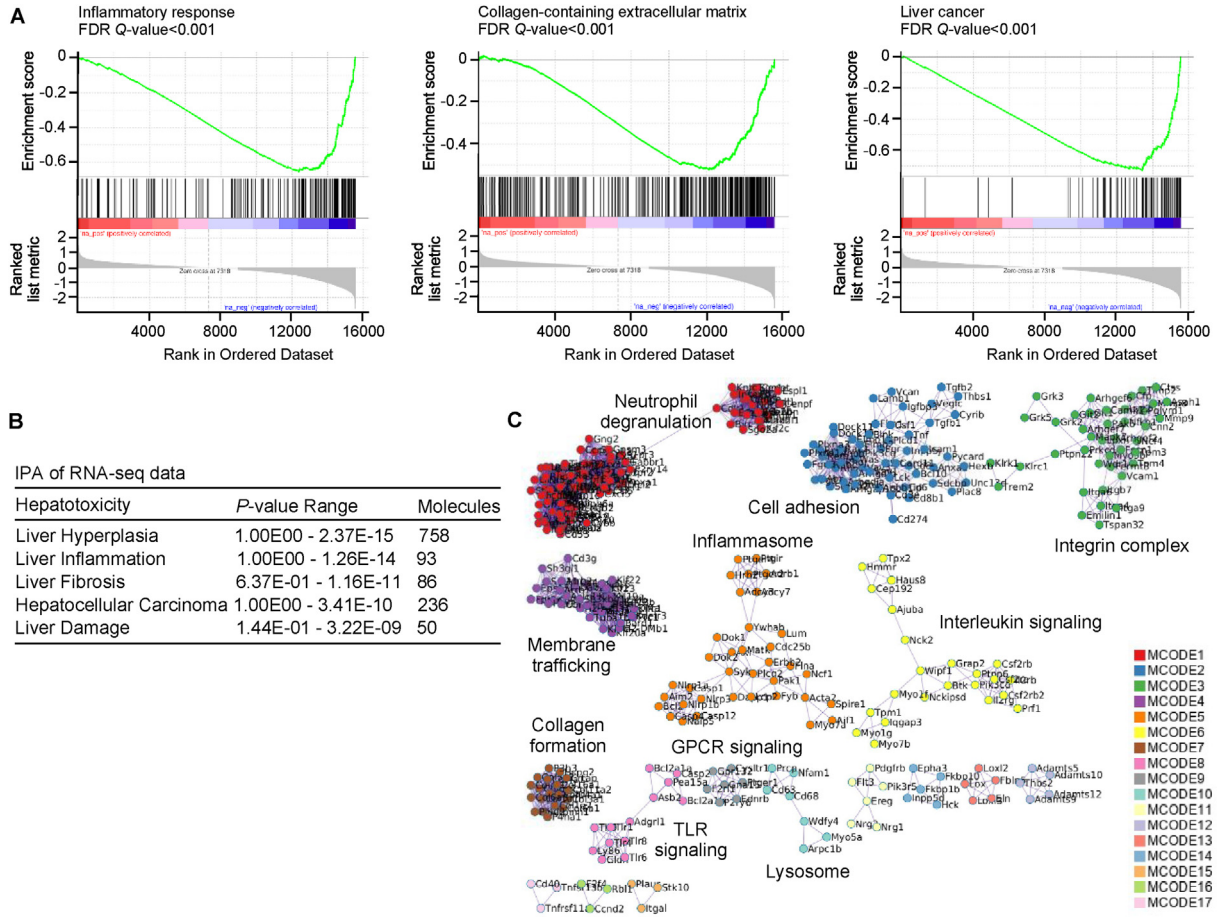

B

IPA of RNA-seq data

Hepatotoxicity	*P*-value Range	Molecules
Liver Hyperplasia	1.00E00 - 2.37E-15	758
Liver Inflammation	1.00E00 - 1.26E-14	93
Liver Fibrosis	6.37E-01 - 1.16E-11	86
Hepatocellular Carcinoma	1.00E00 - 3.41E-10	236
Liver Damage	1.44E-01 - 3.22E-09	50

Figure 3 Bioinformatics analysis of RNA-seq data of aged mice with or without H-VLN treatment. mRNAs of the liver samples from the same animals in Fig. 2 were extracted and subjected to RNA-seq analysis, followed by bioinformatics analyses. $n = 6$/group. (A) GSEA suggested that H-VLN treatment inversely correlated with inflammatory response, fibrosis, and hepatocarcinogenesis. The gene set "collagen-containing extracellular matrix" (MM12425) was used as the indicator of fibrosis because the fibrous scar results from the accumulation of extracellular matrix proteins (mostly crosslinked collagens). The gene set "liver cancer" (MM535) was based on the genes that were highly over-expressed in liver tumors in *Txnip*$^{-/-}$mice, compared to non-tumor hepatic tissues. Any gene set that reached a False Discovery Rate (FDR) *Q*-value<0.1 was considered significantly correlated. (B) IPA of RNA-seq data showed numbers of H-VLN-regulated genes involved in different hepatic conditions. (C) Metascape analysis was used to visualize the PPI networks of H-VLN-inhibited genes, and 17 network components were identified by the MCODE algorithm.

HSCs that mediate hepatic fibrogenesis[45,46]. IHC staining using anti-α-SMA antibody demonstrated wide activation of HSCs in aged control livers, which was largely blunted by H-VLNs (Fig. 5B and D). Correspondingly, expressions of fibrogenic genes, such as *Col1a1, Timp1*, and *Mmp13,* in the livers were inhibited by H-VLN treatment (Fig. 5E).

The majority of HCC (around 90%) arises in inflamed livers[47]. Chronic activation of immune cells and dysregulation of the immune signal milieu, as well as the resulting fibrosis/cirrhosis, are driving factors that accelerate hepatocarcinogenesis and tumor survival. Because one or more nodules were observed in 40% of control aged mice, we suspected that the hepatic microenvironment in our aged mice predisposed them to HCC. Continuous cell death, along with compensatory proliferation, are key processes in hepatocarcinogenesis[48]. First, cell death was assessed using TUNEL staining. Strong TUNEL signals in both inflammatory foci and hepatocytes in aged livers indicated active cell death and liver injury but were significantly reduced in the liver sections of H-VLN-treated mice (Fig. 6A and C). KI67 IHC staining showed active proliferation in control aged livers, but not in H-VLN-treated aged livers (Fig. 6B and D). Transcription analysis further confirmed that expressions of the genes involved in hepatocarcinogenesis, such as *Mki67, Ccnb1*, *Mcm6*, and *Src*, were suppressed by H-VLNs (Fig. 6E). Consistently, IHC staining of proto-oncogene tyrosine-protein kinase SRC showed that H-VLNs suppressed the SRC level in aged livers (Fig. 6F and G). Taken together, all these biochemical and molecular characterizations supported the notion that the hepatic microenvironment in our control aged mice favored hepatocarcinogenesis; however, H-VLNs curtailed the development of such a milieu, likely through their anti-inflammatory activities.

3.6. *H-VLNs were dominantly taken up by macrophages*

To understand the molecular mechanism for hepatoprotective functions of H-VLNs, we first sought to determine the target cells of H-VLNs in the liver. H-VLNs were labeled with lipophilic dye PKH26 (red fluorescence) and given to 24-month-old male C57BL/6J mice through oral gavage. It was challenging to detect a robust fluorescent signal of H-VLNs in the liver sections using the

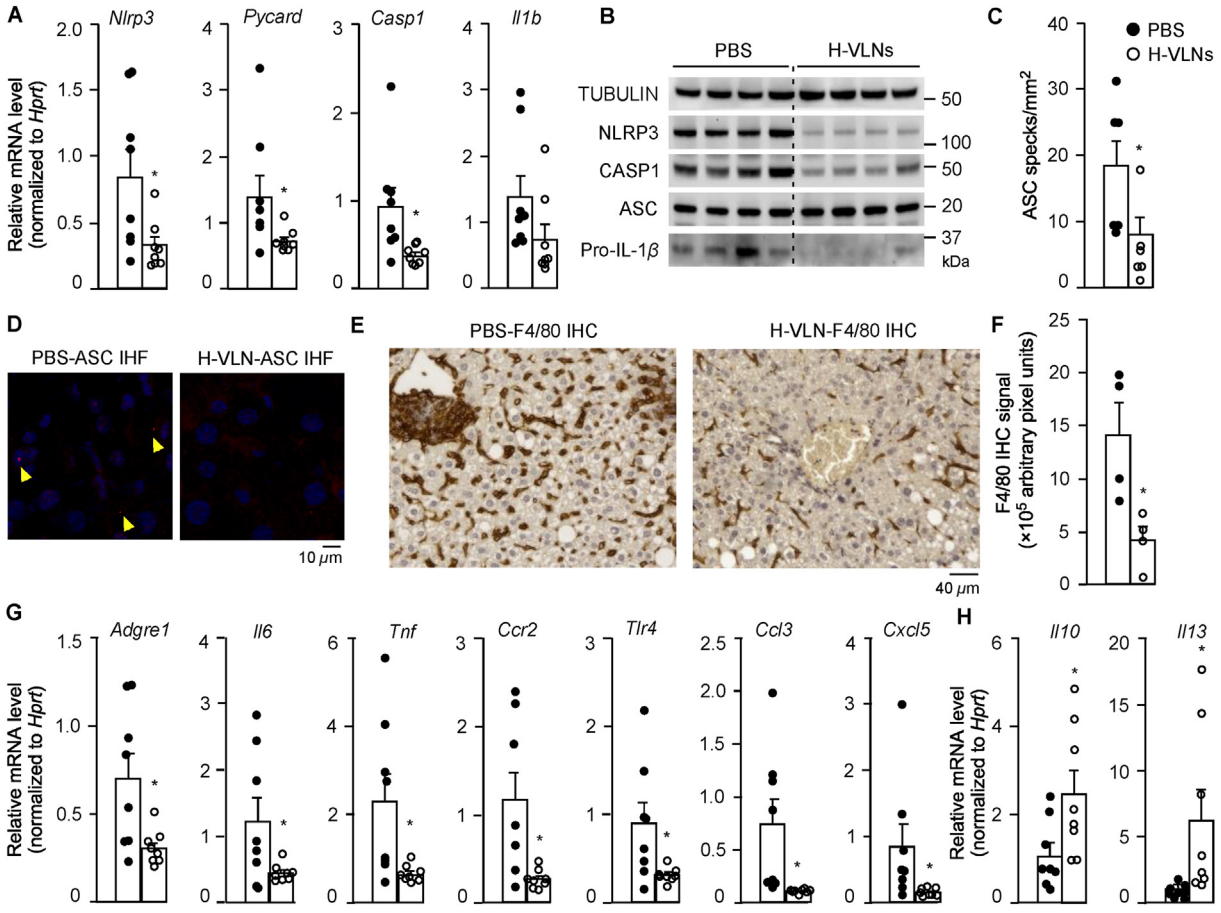

Figure 4 H-VLNs reduced hepatic inflammation in aged mice. The liver samples from the same animals in Fig. 2 were subjected to further analysis. (A) Expression of NLRP3 inflammasome-related genes in mouse livers. $n = 8$/group. (B) Immunoblot analysis of NLRP3 inflammasome-related proteins in mouse livers. $n = 4$/group. (C, D) Representative images (D) and quantification (C) of ASC specks in mouse livers. An anti-ASC antibody was used to conduct IHF staining of liver sections. Upon inflammasome activation, inflammasome subunits oligomerize and form a high-molecular-mass multiprotein complex, which was stained as a single ASC speck in each cell (red dot indicated by yellow arrow). $n = 6$/group. (E, F) Representative images (E) and quantification (F) of F4/80 IHC signal of liver sections. $n = 4$/group. (G—H) Expression of a number of pro-inflammatory genes (G) and anti-inflammatory genes (H) in mouse livers. $n = 8$/group. In the bar graphs, each dot represents one mouse. Data were presented as mean ± SEM, $^*P < 0.05$ and $^{**}P < 0.01$ *vs*. indicated (bar with black dots). Scale bar = 10 or 40 μm.

confocal microscope. Many studies have reported that EVs or dietary VLNs significantly accumulate in the liver after intravenous injection[7,49-51]. Therefore, PHK26-labeled H-VLNs were intravenously given to 24-month-old male C57BL/6J mice daily for three days. The mice were sacrificed on Day 4 to collect liver tissues, and the red fluorescence signal of PKH26-labeled H-VLNs in the liver sections was readily detected under the confocal microscope. These liver sections were subjected to co-localization assays. When the liver samples were co-stained with KERATIN 18 (hepatocyte marker) and F4/80 (the marker of macrophages/Kupffer cells), Most of red signals of H-VLNs were colocalized with F4/80 positive cells (green fluorescence; Fig. 7A). Alternatively, when the liver sections were co-stained with F4/80 and the HSC marker DESMIN, H-VLNs were mainly found in macrophages (Fig. 7B). Lastly, when the liver sections were co-stained with F4/80 and sinusoidal endothelial cell marker CD146, most H-VLNs were found to be accumulated in macrophages (Fig. 7C). Therefore, it seems that H-VLNs were dominantly taken up by macrophages, but not by hepatocytes, HSCs, or sinusoidal endothelial cells in aged livers. To further confirm the inherent target cells of H-VLNs, PKH26-labeled H-VLNs were incubated with BMDMs or Huh7 hepatoma cells. BMDMs readily took up H-VLNs in a dose-dependent manner, but Huh7 took up only a small amount of H-VLNs (Fig. 7D). This *in vitro* experiment confirmed that H-VLNs were inherently and preferentially taken up by macrophages, compared to hepatocytes.

3.7. H-VLNs inhibited C-JUN and NF-κB pathways in aged liver and cultured macrophages

Although the inhibitory effects of H-VLNs on the NLRP3 inflammasome may at least partially explain their anti-inflammatory functions in aged livers, an unbiased bioinformatics analysis of master transcription factors using TRRUST mining was conducted with the RNA-seq data to elucidate possible other targets of H-VLNs. Two transcription factors, C-JUN and NF-κB, were identified as top candidates (Fig. 8A).

C-JUN is a component of the activator protein-1 (AP-1) transcription factors, which are homo- or heterodimers of the JUN (C-JUN, JUNB, and JUND) and FOS (C-FOS, FOSB, FRA1, and

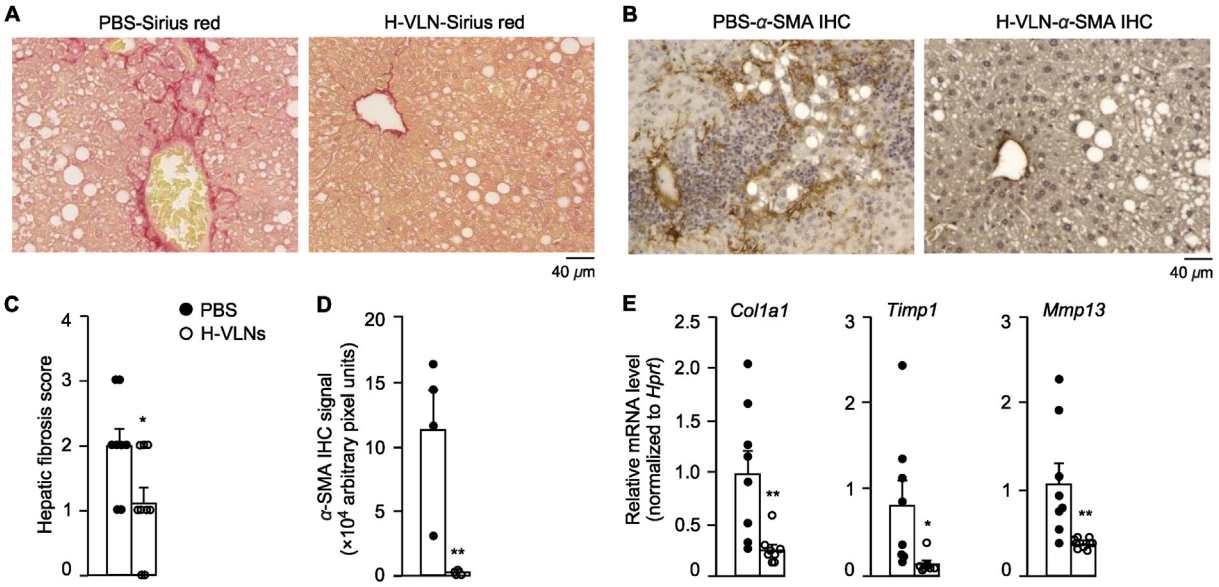

Figure 5 H-VLNs suppressed the development of liver fibrosis in aged mice. The liver samples from the same animals in Fig. 2 were subjected to further analysis. (A) Representative images of Sirius red collagen staining of liver sections showing hepatic fibrosis. (B) Representative images of α-SMA IHC of liver sections. (C) Fibrosis score of mouse livers. The tissues stained with Sirius red were scored for hepatic fibrosis (stages 0−4). When multiple mice were ranked in the same stage, their dots were spread out horizontally. $n = 8-9$/group. (D) Quantification of α-SMA IHC signal of liver sections. $n = 4$/group. (E) Expression of fibrogenic genes in livers. $n = 8$/group. In the bar graphs, each dot represents one mouse. Data were presented as mean ± SEM. $^*P < 0.05$ and $^{**}P < 0.01$ *vs.* indicated (bar with black dots). Scale bar = 40 μm.

FRA2) proteins and mediate the expression of genes involved in cell death, proliferation, differentiation, and immune response[52,53]. The JNKs are the upstream activators of C-JUN. In response to diverse stimuli including cytokines, JNKs are phosphorylated and become activated. Activated JNKs phosphorylate C-JUN at serine residues 63 and 73, thus enhancing its transcriptional activity. The phosphorylated C-JUN subsequently induces its own transcription and expression of other target genes. The levels of phosphorylated JNK, total C-JUN, and phosphorylated C-JUN were much higher in the control livers than in those from the H-VLN-treated group (Fig. 8B), suggesting that C-JUN signaling was suppressed by H-VLNs in aged livers.

NF-κB is a family of master transcription factors that regulate the transcription of more than 500 genes involved in cell survival, tissue renewal, and inflammation[54]. This family includes NF-κB1 (P50), NF-κB2 (P52), RELA (P65), RELB, and C-REL. In resting cells, NF-κB is bound by the IκB proteins, among which IκBα is the most prominent member. This binding masks the nuclear localization site of NF-κB and thus sequesters NF-κB in the cytoplasm. In response to canonical stimuli, such as IL-1, IκBα is phosphorylated and degraded, leading to the release of NF-κB family members and resulting in their rapid and transient nuclear translocation in the predominant forms of P50/P65 and P50/C-REL dimers. In our aged mice, the hepatic IκBα level was higher in H-VLN-treated mice compared to the control mice (Fig. 8B), indicating that NF-κB was likely to be less active in H-VLN-treated animals. P65 IHC staining showed that P65 was highly expressed and dominantly located in the nuclei of many immune cells in the control livers, but its level was much lower in the livers of H-VLN-treated mice (Fig. 8C and D).

Since H-VLNs were dominantly taken up by macrophages in aged livers, the direct effects of H-VLNs on C-JUN and NF-κB were further assessed in cultured macrophages. First, increasing amounts of H-VLNs were incubated with BMDMs for 16 h to assess their possible cytotoxicity. For the doses ($0.5-40 \times 10^9$/mL) we tested, H-VLNs did not show any cytotoxicity on cultured primary macrophages (Supporting Information Fig. S7A). Next, H-VLNs ($0.5-4.5 \times 10^9$/mL) were incubated with BMDMs for 16 h, followed by LPS treatment to activate both C-JUN and NF-κB. LPS induces transient degradation of IκBα, which was dose-dependently inhibited by H-VLNs (Fig. 9A). Consistently, the nuclear translocation of P65 was largely curbed by H-VLNs (Fig. 9B, top panels). As a consequence, the well-known target genes of NF-κB, such as *Tnf*, *Il6*, and *Nlrp3*, were suppressed by H-VLN treatment (Fig. 9C). Together, these results indicated that NF-κB activation was inhibited by H-VLNs in primary macrophages. Similarly, JNK phosphorylation and subsequent C-JUN phosphorylation induced by LPS were suppressed by H-VLNs (Fig. 9A). IF staining using anti-phosphorylated C-JUN antibody confirmed that H-VLNs remarkably reduced the level of phosphorylated C-JUN in the nuclei (Fig. 9B, bottom panels). The expression of the C-JUN target *Cox2* gene[55] was down-regulated by H-VLNs (Fig. 9D). Thus, H-VLNs also strongly suppressed the transcription activity of C-JUN in BMDMs.

3.8. *Biomolecules in H-VLNs were identified to inhibit C-JUN and NF-κB pathways*

H-VLNs were heated at 95 °C for 10 min to denature their proteins. As shown by negative stain TEM images (Fig. S7B), heated H-VLNs showed a membrane-enclosed vesicular structure similar to that of untreated or regular H-VLNs. The TEM images of sonicated H-VLNs served as a positive control showing the disrupted vesicular structure of H-VLNs. Our previous study[15] showed that this heat treatment (95 °C for 10 min) effectively abolished the functions of protein cargos in EVs. Notably, such heated H-VLNs retained their ability to prevent IκBα degradation and JNK phosphorylation (Fig. 10A), indicating that proteins in

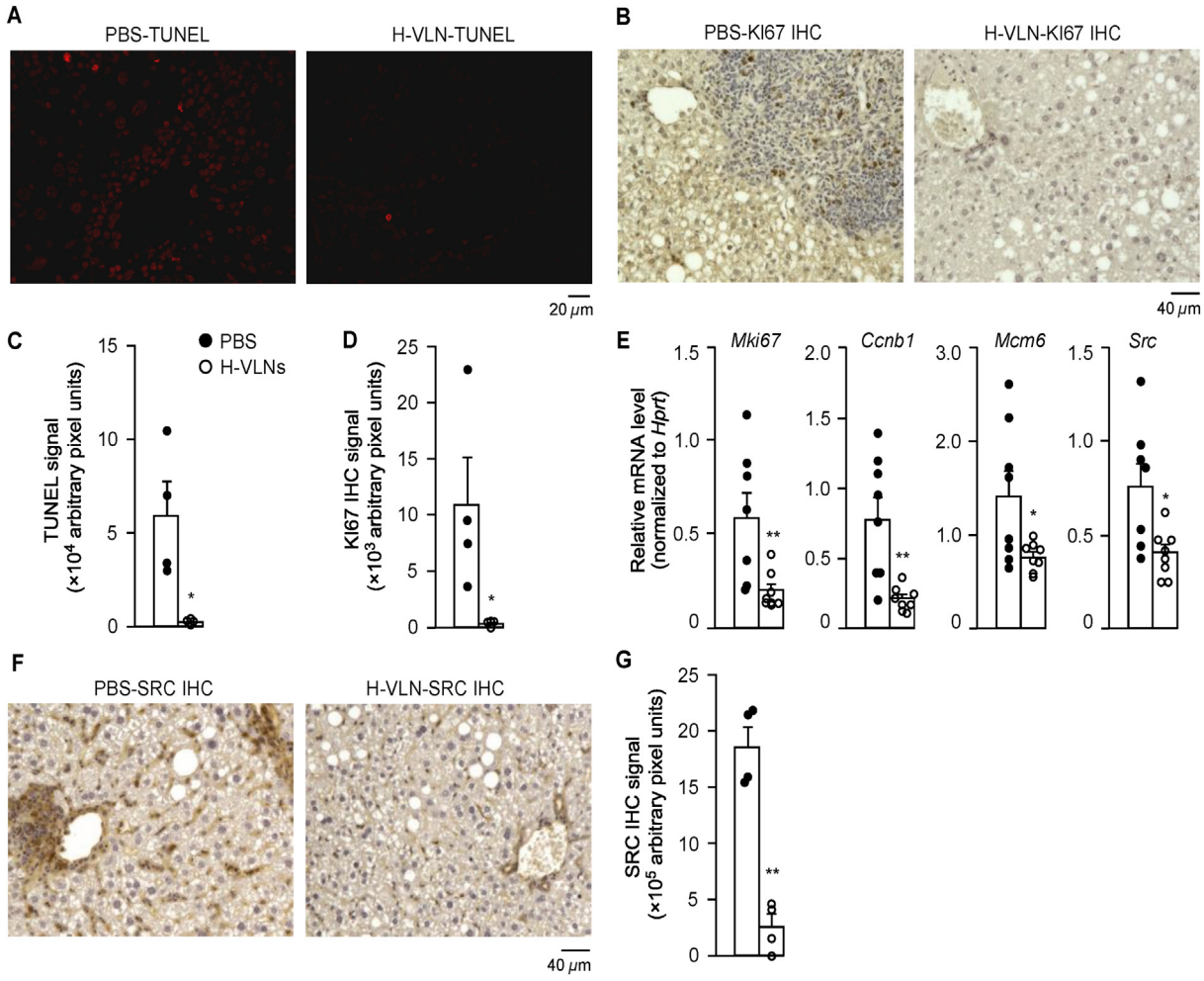

Figure 6 Favored hepatocarcinogenesis in aged mice was curtailed by H-VLN treatment. The liver samples from the same animals in Fig. 2 were subjected to further analysis. (A) Representative images of TUNEL staining of liver sections. (B) Representative images of KI67 IHC of liver sections. (C) Quantification of TUNEL signal of liver sections. $n = 4$/group. (D) Quantification of KI67 IHC signal of liver sections. $n = 4$/group. (E) Expression of hepatic genes involved in hepatocarcinogenesis. $n = 8$/group. (F and G) Representative images (F) and quantification (G) of SRC IHC signal of liver sections. $n = 4$/group. In the bar graphs, each dot represents one mouse. Data were presented as mean ± SEM. $^{*}P < 0.05$ and $^{**}P < 0.01$ *vs*. indicated (bar with black dots). Scale bar = 20 or 40 μm.

H-VLNs were not essential to inhibit both NF-κB and C-JUN pathways. Total RNAs were extracted from H-VLNs and directly transfected into primary macrophages. These RNAs from H-VLNs dose-dependently inhibited both IκBα degradation and JNK phosphorylation (Fig. 10B), suggesting that RNAs in H-VLNs were important in mediating the inhibitory effects on NF-κB and C-JUN signaling. In our previous study[6], RNA deep sequencing was conducted with RNAs from H-VLNs, and 3,444,167 quality reads were obtained. Using miRDeep2 analysis, we mapped these reads to the entire miRbase sequence library (version 22) with stringent mapping criteria (allowing 0 mismatch for precursor sequence mapping and ≤1 mismatch for mature sequence mapping using Bowtie). This analysis resulted in the identification of 14 unique miRNAs in H-VLNs[6]. Among these, the top five most abundant miRNAs (miR5119, miR2478, miR1582, miR5108, and miR156a) were selected for further tests. The mimics of these five miRNAs were purchased and individually transfected into BMDMs. Remarkably, only miR5119 and miR5108, but not the other three miRNAs from H-VLNs were found to strongly inhibit transcription of the *Il6* gene without suppressing expression of the *Tnf, Nlrp3,* or *Cox2* genes (Fig. 10C and Fig. S8A). Dose tests confirmed that both miR5119 and miR5108 inhibited *Il6* expression in a dose-dependent manner (Fig. S8B and S8C).

Finally, H-VLNs were subjected to chloroform/methanol extraction to separate fractions soluble in chloroform (C-fraction) and soluble in a water and methanol mixture (WM-fraction). As shown in Fig. 10D, the C-fraction showed no effects, whereas the WM-fraction strongly inhibited both NF-κB and C-JUN signaling. Because phenolic compounds with anti-inflammatory functions are among the well-established components in honey[5], the WM-fraction of H-VLNs was subjected to phenolic compound analysis using LC-MS. The top five most abundant phenolic compounds were luteolin, syringic acid, vanillic acid, protocatechuic acid, and *p*-coumaric acid (Supporting Information Fig. S9A). Among them, only luteolin suppressed the expression of the *Il6*

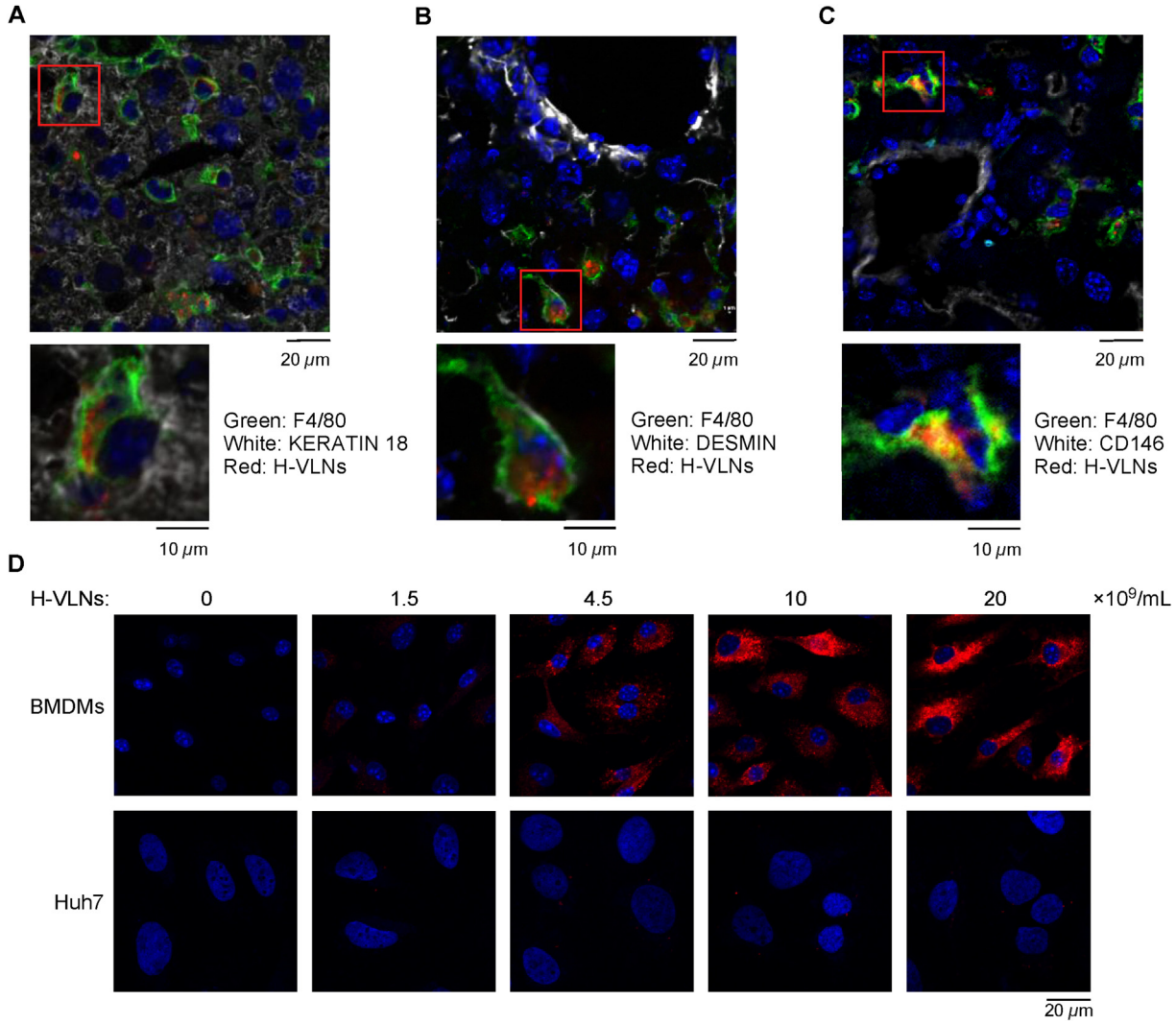

Figure 7 H-VLNs were dominantly taken up by macrophages. (A–C) H-VLNs were labeled with a lipophilic dye PKH26. The labeled H-VLNs were intravenously injected at 600 fluorescence intensity/g into 2-year-old male C57BL/6J mice daily for 3 days. The animals were sacrificed on Day 4 and the livers were frozen in O.T.C. solution. (A) Representative images of IHF staining using anti-F4/80-Alexa Fluor 488 antibody and anti-KERATIN 18 antibody. (B) Representative images of IHF staining using anti-F4/80-Alexa Fluor 488 antibody and anti-DESMIN antibody. (C) Representative images of IHF staining using anti-F4/80-Alexa Fluor 488 antibody and anti-CD146-APC antibody. (D) H-VLNs were readily taken up by BMDMs, but not by Huh7 cells. BMDMs or Huh7 cells were incubated with 1.5–20 × 10^9/mL of PKH26-labeled H-VLNs for 16 h. After extensive washing, the cells were fixed using 4% paraformaldehyde, and their images were taken using confocal microscopy. In all the images, nuclei were stained using SYTOX deep red dye and shown in blue. Scale bar = 10 or 20 μm.

and *Cox2* genes, but not the *Tnf* or *Nlrp3* genes (Fig. 10E and Fig. S9B). Our results were consistent with a previous report showing the inhibitory effects of luteolin on the *Il6* transcription in microglia[56]. Further dose experiments showed that luteolin dose-dependently inhibited transcription of both the *Il6* and *Cox2* genes (Fig. S9C). Cotreatment with luteolin, miR5108, and miR5119 led to synergistic inhibitory effects on IκBα degradation, JNK phosphorylation, and transcription of the *Il6* and *Cox2* genes (Fig. 10F and Fig. S9D). Taken together, miR5108, miR5119, and luteolin were identified as active biomolecules in H-VLNs that inhibited both C-JUN and NF-κB signaling.

4. Discussion

In summary, H-VLNs taken orally were found to protect livers from chronic inflammation, as well as inhibiting further development of fibrosis and nodule formation in naturally aged mice. H-VLNs were dominantly taken up by Kupffer cells in the liver and suppressed the NLRP3 inflammasome, C-JUN, and NF-κB pathways. The miRNAs miR-5119 and miR5108 and the phenolic compound luteolin in H-VLNs were identified to suppress the activation of C-JUN and NF-κB signaling.

NAFLD has become the most prevalent liver disease worldwide, with the highest incidence in the senile population[2,3]. NASH, the advanced form of NAFLD, has emerged as a leading cause of liver failure-related transplantation and death. Despite the high prevalence and potential severe clinical consequences of NAFLD/NASH, no specific licensed medications are available to treat them. Some medications have entered phase II and/or III clinical trials to treat NASH patients. In NASH clinical trials, patients are often evaluated using two endpoints: NASH resolution with no worsening of fibrosis and fibrosis improvement with no

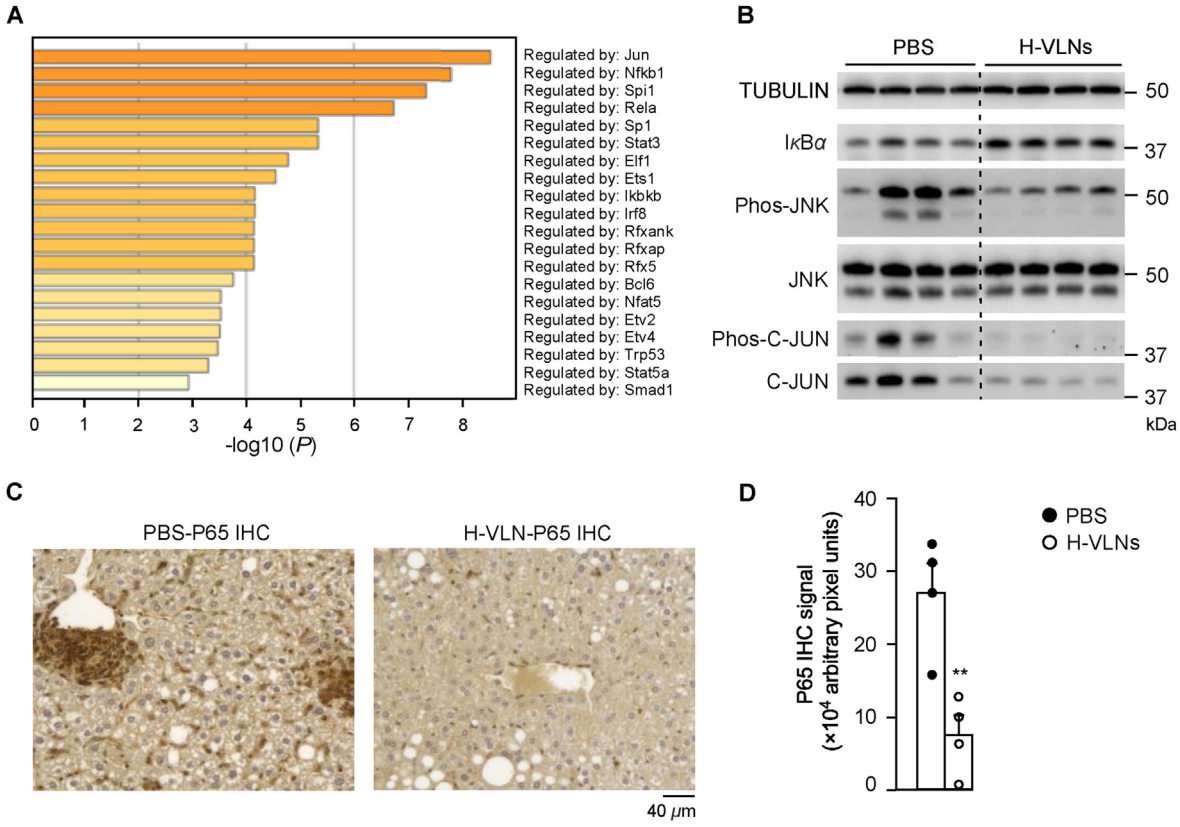

Figure 8 H-VLNs inhibited activation of C-JUN and NF-κB pathways in the aged liver. The liver samples from the same animals in Fig. 2 were used for further analysis. (A) Bioinformatics analysis of RNA-seq data using TRRUST mining indicated transcription factors regulated by H-VLNs. $n = 6$/group. (B) Immunoblot analysis of key proteins involved in NF-κB and C-JUN signaling pathways. $n = 4$/group. (C−D) Representative images (C) and quantification (D) of P65 IHC signal of liver sections. $n = 4$/group. In the bar graphs, each dot represents one mouse. Data were presented as mean ± SEM. $^{*}P < 0.05$ and $^{**}P < 0.01$*vs*. indicated (bar with black dots). Scale bar = 40 μm.

worsening of NASH. A 6-month phase IIb trial with lanifibranor, a pan-peroxisome proliferator-activated receptor (PPAR) agonist, demonstrated that this medication met both endpoints[57]. However, patients treated with lanifibranor experienced more frequent weight gain, diarrhea, nausea, peripheral edema, and anemia compared to patients who received a placebo. A phase III clinical trial for lanifibranor is currently underway and is expected to be completed in 2026[58]. A phase III clinical trial of 1968 patients treated with obeticholic acid, an agonist of farnesoid X receptor (FXR) was completed in September of 2023. An 18-month interim analysis from this clinical trial showed that the medicine met the endpoint of fibrosis improvement, but not the endpoint of NASH resolution[59]. The most common adverse event related to the use of obeticholic acid was mild to moderate pruritus. Although the results of clinical trials with these medications are promising, the reported treatment duration is relatively short in patients (a few months to 1.5 years). The long-term safety, efficacy, and associated side effects of these medications need to be further assessed. While physical activities and dietary changes comprise the first-line approach to NAFLD management, elderly people are limited in adapting to these behaviors due to aging-associated digestive functional decline and frailty. It also becomes increasingly challenging for geriatric patients to handle the adverse side effects of medications, as well as the perioperative risk of liver transplantation. Therefore, new interventions, especially those that are feasible and friendly to an elderly population, are critically needed to address this global health problem.

The naturally aged mice in our study spontaneously developed hepatic steatosis, inflammation, fibrosis, and nodules. The pathohistological assessment of aged livers showed that their average NAS (3.8 ± 0.4) was comparable to the NAS levels (ranging from 3 to 5) of NASH mouse models induced by feeding with a high-fat, -cholesterol, and -fructose/sucrose diet for 3−6 months[35,37,38]. The bioinformatic analyses of RNA-seq data also suggested that aged livers underwent extensive transcriptional activation of genes involved in steatosis, inflammation, fibrosis, and HCC, compared to young livers, further supporting that NASH development occurred in the aged mice at the molecular level. Remarkably, weekly oral administration of H-VLNs to these aged mice for one year significantly alleviated chronic inflammation and inhibited further development of fibrosis and nodule formation in their livers. Thus, oral intake of H-VLNs regularly could serve as an easy and user-friendly new intervention to curb the development of NASH.

Honey has been reported to protect the liver from insults. One study reported that honey alleviated liver damage in rats induced by *N*-ethylmaleimide or metanil yellow[60,61]. Daily oral administration of honey reduced steatosis, inflammation, and fibrosis in high-fat diet-induced NAFLD in rats[62]. A recent cross-sectional study of 22,979 adults aged 20−90 years indicated that honey intake (2−6 times/week) inversely correlated with NAFLD incidence, but excess honey intake (≥1 times/day) led to little protection from NAFLD (possibly due to excess sugar intake)[63]. Indeed, the high sugar content of honey is a concern, considering

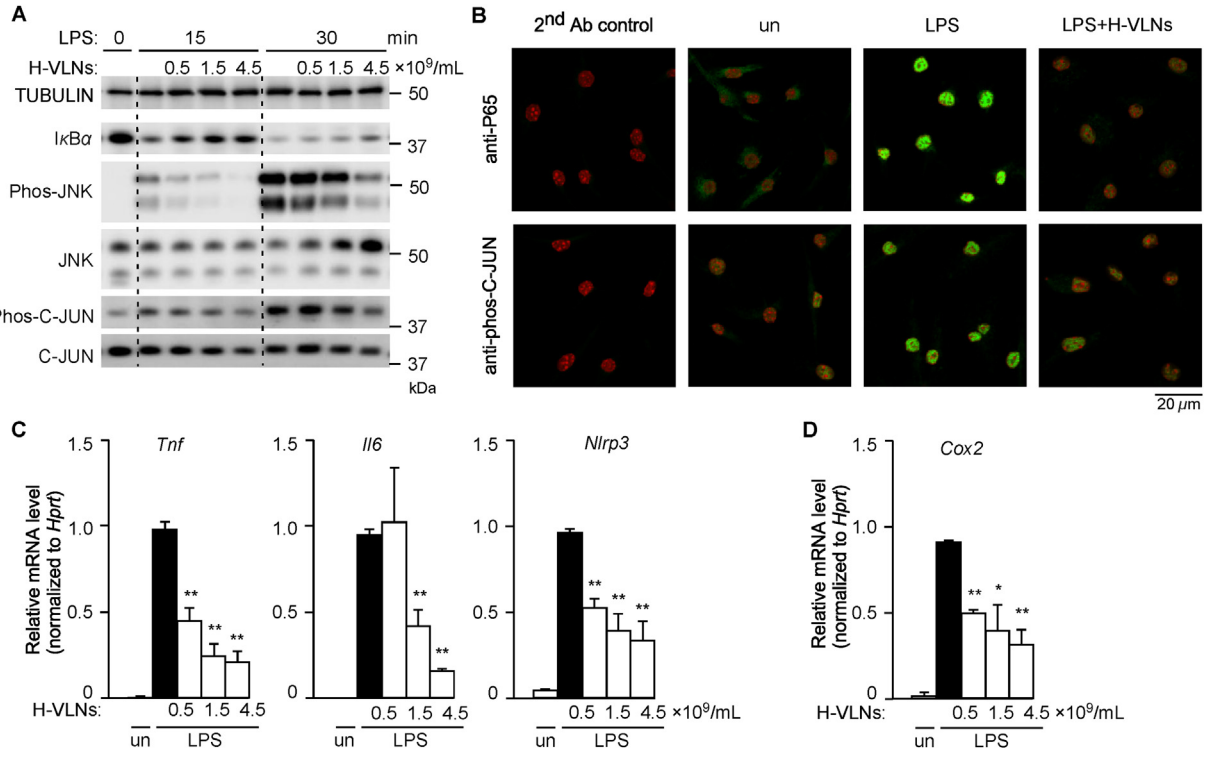

Figure 9 H-VLNs inhibited C-JUN and NF-κB pathways in BMDMs. BMDMs were treated with 0.5−4.5 × 10^9/mL of H-VLNs for 16 h, followed by LPS incubation for 15−30 min (A), 15 min (B), or 3 h (C, D). The untreated (un) cells were used as a negative control for LPS treatment. Cells were harvested for further analysis. (A) H-VLNs inhibited IκBα degradation, JNK phosphorylation, and C-JUN phosphorylation in BMDMs challenged with LPS. TUBULIN was a loading control. (B) H-VLNs inhibited nuclear translocation of P65 or phosphorylation of C-JUN induced by LPS. 4.5 × 10^9/mL of H-VLNs were used. (C) H-VLNs suppressed the expression of the NF-κB target genes. (D) H-VLNs reduced the expression of the C-JUN target gene. Data were presented as mean ± SEM. *$P < 0.05$ and **$P < 0.01$ compared with BMDMs treated with LPS alone (black bar). Scale bar = 20 μm.

clinical evidence that daily intake of honey for two months led to the elevation of blood hemoglobin A1c in diabetic patients[64,65]. Extraction of H-VLNs from honey removes sugars and possible agrochemical contaminants, and the resulting nanoparticles have demonstrated remarkable anti-inflammatory functions and strong protection for the aged liver. Therefore, H-VLNs present a brand-new sugar-free derivative of honey with the promising potential of curtailing NASH progression.

The well-established constituents in honey, such as vitamins, minerals, or polyphenols, have been considered to be its main bioactive components[66]. In the current study, we found that oral intake of a recently identified honey component, H-VLNs, suppressed chronic hepatic inflammation and protected the aged liver from the development of NASH. These newly identified hepatoprotective functions of H-VLNs may, at least partially, provide a mechanistic explanation for the reported beneficial effects on the liver of honey intake. Furthermore, we found that H-VLNs inherently targeted Kupffer cells in the liver and suppressed NLRP3 inflammasome activation and activities of two inflammatory master transcript factors, C-JUN and NF-κB. In addition, miR5119, miR5108, and luteolin in H-VLNs were identified to synergistically inhibit C-JUN and NF-κB pathways. Thus, our study provides unprecedented mechanistic insights into how biomolecules carried by H-VLNs in honey target specific tissue cells, mediate a series of inflammatory signaling pathways, and carry out protective functions in the liver. Such new mechanistic insights would significantly improve our understanding of how honey exerts beneficial functions in humans, fundamentally altering how people think of, process, and use honey.

Genetic evidence has supported the notion that dysregulated activation of C-JUN, NF-κB, and the NLRP3 inflammasome play causal roles in the development of NASH. Activation of C-JUN and NF-κB, accompanied by the increased expression of their target inflammatory genes, has been observed in various NASH animal models[67-69] and NASH patients[67,70-72]. Deletion of the *Rela* (encoding P65) or *Jun* (encoding C-JUN) gene led to embryonic lethality with massive apoptosis in livers[73,74], pointing to the essential functions of NF-κB and C-JUN during liver development. Genetic inactivation of the *Jnk1* gene (encoding JNK1, an upstream activator of C-JUN) decreased C-JUN phosphorylation, hepatic inflammation, and liver injury induced by a methionine- and choline-deficient diet (MCD)[69]. Hepatic overexpression of nondegradable IκB (upstream sequester of NF-κB) successfully blocked MCD-induced NF-κB activation in the liver[68]. This genetic blockade of NF-κB signaling decreased neither the hepatic triacylglycerol level nor steatosis score, but significantly ameliorated hepatic inflammation and liver injury induced by MCD feeding[68]. Conversely, when a constitutively active form of the *Ikbkb* gene [encoding IκB kinase β (IKKβ) protein, upstream activator of NF-κB] was inducibly expressed in the liver, the IKK complex phosphorylated the IκB proteins and promoted their degradation, leading to activation of NF-κB, hepatic inflammation,

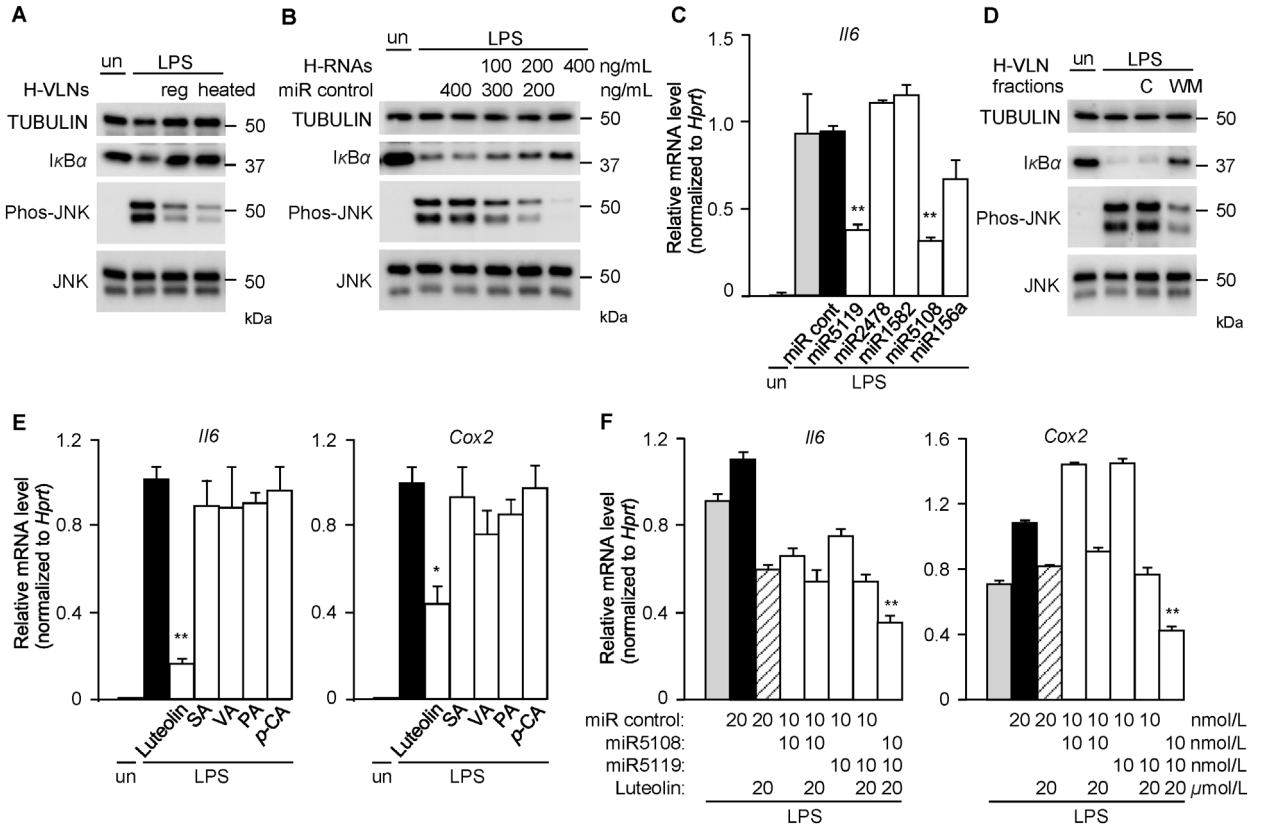

Figure 10 miR5119, miR5108, and luteolin in H-VLNs inhibited C-JUN and NF-κB signaling in BMDMs. BMDMs were incubated with H-VLNs, their fractions, or chemical compounds for 16 h. Alternatively, BMDMs were transfected with H-VLN RNAs or individual miRNA mimic. Afterward, LPS was added to the cells for 15 min (A, B and D) or 3 h (C, E, and F). Cells were harvested for immunoblot or mRNA analysis. un: untreated BMDMs. (A) Proteins in H-VLNs were not critical in mediating the inhibitory effects of H-VLNs on C-JUN and NF-κB pathways. reg: regular H-VLNs. heated: H-VLNs were heated at 95 °C for 10 min to denature proteins. 1.5×10^9/mL of H-VLNs were used. (B) Total RNAs from H-VLNs (H-RNAs) inhibited both NF-κB and C-JUN pathways. 100−400 ng/mL of H-VLN RNAs, along with different amounts of miRNA (miR) control AllStars negative control siRNA, were transfected in BMDMs to ensure total transfected RNAs of 400 ng/mL. (C) miR5119 and miR5108 inhibited transcription of the *Il6* gene. 20 nmol/L of miR control or individual miRNA mimic was transfected. miR cont: miR control. (D) WM-fraction of H-VLNs inhibited IκBα degradation and JNK phosphorylation. H-VLNs were subjected to chloroform/methanol extraction. 2.5% of the fraction soluble in chloroform (C-fraction) or the fraction soluble in water and methanol mixture (WM-fraction) was incubated with BMDMs. (E) Luteolin inhibited the expression of the *Il6* and *Cox2* genes. 20 μmol/L of each compound was used. SA: syringic acid; VA: vanillic acid; PA: protocatechuic acid; *p*-CA: *p*-coumaric acid. (F) Co-treatment of luteolin, miR5119, and miR5108 synergistically inhibited the expression of the *Il6* and *Cox2* genes. Data were presented as mean ± SEM. $^*P < 0.05$ and $^{**}P < 0.01$ compared with BMDMs treated with LPS and negative miR control (black bar in C), or LPS alone (black bar in E), or LPS, negative miR control, and luteolin (striped-line bar in F).

and spontaneous development of liver fibrosis[75]. Similar to C-JUN and NF-κB, expression of the subunit components of the NLRP3 inflammasome and its activity are significantly elevated in mouse NASH models and NASH patients[76-78]. Genetic ablation of the *Nlrp3* or *Casp1* gene in mice typically protected mice from diet-induced NASH, as demonstrated by attenuated liver injury, inflammation, and fibrosis[77,79,80]. Tamoxifen-inducible expression of the hyperactive $NLRP3^{A350V}$ mutant protein led to the spontaneous development of inflammation and fibrosis in the liver[81]. In a study of wildtype (wt) and $Nlrp3^{-/-}$ mice[82], the livers from aged wt mice also displayed steatosis, inflammation, and fibrosis, similar to the phenotypes of our aged mice. The study results did not mention whether any nodule formation was observed in the aged wt livers. Remarkably, deletion of the *Nlrp3* gene alleviated aging-associated hepatic inflammation and fibrosis[82].

In this study, orally administered H-VLNs were dominantly taken up by Kupffer cells in the liver, reducing activities of the NLRP3 inflammasome, C-JUN signaling, and NF-κB pathway and, by doing so, curtailing hepatic inflammation in aged mice. Considering the causal role of chronic inflammation in the development of hepatic fibrosis and HCC[44,47], we reasoned that this suppression of hepatic inflammation by H-VLNs abrogated further development of fibrosis and hepatocarcinogenesis in aged mice. Our findings, in agreement with previous results of genetic studies, provide compelling evidence that simultaneous suppression of the NLRP3 inflammasome, C-JUN, and NF-κB pathways in Kupffer cells in the liver is an effective modality to suppress hepatic chronic inflammation and more advanced conditions such as fibrosis and HCC. This evidence would ultimately promote the idea of developing new interventions that concomitantly target these key inflammatory mediators in Kupffer cells in the management of NASH.

Of note, a previous study showed that daily oral administration of honey not only reduced inflammation and fibrosis in high-fat

diet-induced NAFLD in rats but also suppressed steatosis and expression of lipogenic genes in the liver[62]. In our study, weekly oral administration of H-VLNs in aged mice affected neither steatosis nor lipogenic gene expression. Further studies are warranted to assess whether adjustment of administration frequency or dose of H-VLNs further inhibits steatosis. It would also be interesting to evaluate the hepatoprotective functions of H-VLNs in diet-induced NAFLD/NASH animal disease models and eventually in NAFLD/NASH patients. Another intriguing direction is to load these anti-inflammatory biomolecules identified from H-VLNs into nanoparticles to develop nanodrugs with well-defined compositions and assess their potential hepatoprotective functions in NASH disease models.

Acknowledgments

This work was supported by the United States Department of Agriculture (USDA) National Institute of Food and Agriculture (NIFA) Multistate Hatch Project 1021080, Standard Grant (2021-67017-34206, USA), and the National Institutes of Health (NIH) grant R01DK124590 (USA). The authors acknowledge the use of the Morrison Microscopy Core Research Facility, Veterinary Diagnostic Laboratory, Proteomics and Metabolomics Facility, and the Biomedical and Obesity Research Core (BORC) of the Nebraska Center for the Prevention of Obesity Diseases through Dietary Molecules (NPOD) at the University of Nebraska−Lincoln, and the Genomics Core Facility and Bioinformatics and Systems Biology Core Facility at the University of Nebraska Medical Center. Morrison Microscopy Core Research Facility was partially funded by the Nebraska Center for Integrated Biomolecular Communication COBRE grant (P20 GM113126, NIGMS, USA) and the Nebraska Research Initiative.

Author contributions

Jiujiu Yu conceived and supervised the project. Baolong Liu, Phuong Linh Nguyen, and Jiujiu Yu designed the experiments. Baolong Liu, Phuong Linh Nguyen, and Han Yu, with the help of Xingzhi Li, Huiren Wang, and Tram Gia Bao Nguyen, conducted the experiments and analyzed the data. Prakash Kumar Sahoo and Sathish Kumar Natarajan provided their expertise for hepatic biochemical studies. Meghna Sur and Jay Reddy contributed to nanoparticle characterization. Sarah Sillman conducted pathological analyses and grading of liver sections. Stephen D. Kachman and Guoqing Lu conducted bioinformatics and statistical analyses. Bara Altartouri contributed to transmission electron microscopy studies. Mahesh Pattabiraman conducted the compound identification experiments. Jiujiu Yu, Baolong Liu, Phuong Linh Nguyen, and Mahesh Pattabiraman wrote and revised the manuscript with the help of other coauthors. All of the authors have read and approved the final manuscript.

Conflicts of interest

The authors declare no conflicts of interest.

Appendix A. Supporting information

Supporting information to this article can be found online at https://doi.org/10.1016/j.apsb.2024.05.002.

References

1. Sheka AC, Adeyi O, Thompson J, Hameed B, Crawford PA, Ikramuddin S. Nonalcoholic steatohepatitis: a review. *JAMA* 2020;**323**:1175−83.
2. Alqahtani SA, Schattenberg JM. NAFLD in the elderly. *Clin Interv Aging* 2021;**16**:1633−49.
3. Younossi ZM, Golabi P, Paik JM, Henry A, Van Dongen C, Henry L. The global epidemiology of nonalcoholic fatty liver disease (NAFLD) and nonalcoholic steatohepatitis (NASH): a systematic review. *Hepatology* 2023;**77**:1335−47.
4. Younossi ZM, Corey KE, Lim JK. AGA clinical practice update on lifestyle modification using diet and exercise to achieve weight loss in the management of nonalcoholic fatty liver disease: expert review. *Gastroenterology* 2021;**160**:912−8.
5. Bogdanov S, Jurendic T, Sieber R, Gallmann P. Honey for nutrition and health: a review. *J Am Coll Nutr* 2008;**27**:677−89.
6. Chen X, Liu B, Li X, An TT, Zhou Y, Li G, et al. Identification of anti-inflammatory vesicle-like nanoparticles in honey. *J Extracell Vesicles* 2021;**10**:e12069.
7. Liu B, Li X, Yu H, Shi X, Zhou Y, Alvarez S, et al. Therapeutic potential of garlic chive-derived vesicle-like nanoparticles in NLRP3 inflammasome-mediated inflammatory diseases. *Theranostics* 2021;**11**:9311−30.
8. Pourcet B, Zecchin M, Ferri L, Beauchamp J, Sitaula S, Billon C, et al. Nuclear receptor subfamily 1 group D member 1 regulates circadian activity of NLRP3 inflammasome to reduce the severity of fulminant hepatitis in mice. *Gastroenterology* 2018;**154**:1449−1464 e20.
9. Li X, Li C, Zhang W, Wang Y, Qian P, Huang H. Inflammation and aging: signaling pathways and intervention therapies. *Signal Transduct Targeted Ther* 2023;**8**:239.
10. Franceschi C, Garagnani P, Parini P, Giuliani C, Santoro A. Inflammaging: a new immune-metabolic viewpoint for age-related diseases. *Nat Rev Endocrinol* 2018;**14**:576−90.
11. Latz E, Duewell P. NLRP3 inflammasome activation in inflammaging. *Semin Immunol* 2018;**40**:61−73.
12. Shaw AC, Goldstein DR, Montgomery RR. Age-dependent dysregulation of innate immunity. *Nat Rev Immunol* 2013;**13**:875−87.
13. Natarajan SK, Stringham BA, Mohr AM, Wehrkamp CJ, Lu S, Phillippi MA, et al. FoxO3 increases *miR-34a* to cause palmitate-induced cholangiocyte lipoapoptosis. *J Lipid Res* 2017;**58**:866−75.
14. Wang Q, Yu J, Kadungure T, Beyene J, Zhang H, Lu Q. ARMMs as a versatile platform for intracellular delivery of macromolecules. *Nat Commun* 2018;**9**:960.
15. Liu B, Nguyen PL, Yu H, Li X, Wang H, Price J, et al. Critical contributions of protein cargos to the functions of macrophage-derived extracellular vesicles. *J Nanobiotechnol* 2023;**21**:352.
16. Vu DC, Alvarez S. Phenolic, Carotenoid and saccharide compositions of Vietnamese camellia sinensis teas and herbal teas. *Molecules* 2021;**26**.
17. Liang W, Menke AL, Driessen A, Koek GH, Lindeman JH, Stoop R, et al. Establishment of a general NAFLD scoring system for rodent models and comparison to human liver pathology. *PLoS One* 2014;**9**:e115922.
18. Kleiner DE, Brunt EM, Van Natta M, Behling C, Contos MJ, Cummings OW, et al. Design and validation of a histological scoring system for nonalcoholic fatty liver disease. *Hepatology* 2005;**41**:1313−21.
19. Chen X, Zhou Y, Yu J. Exosome-like nanoparticles from ginger rhizomes inhibited NLRP3 inflammasome activation. *Mol Pharm* 2019;**16**:2690−9.
20. Liu B, Lu Y, Chen X, Muthuraj PG, Li X, Pattabiraman M, et al. Protective role of shiitake mushroom-derived exosome-like nanoparticles in D-galactosamine and lipopolysaccharide-induced acute liver injury in mice. *Nutrients* 2020;**12**:477.
21. Andrew S. FastQC: a quality control tool for high throughput sequence data. Available from: http://wwwbioinformaticsbabrahamacuk/projects/fastqc/2010.

22. Gordon A. FASTQ/A short-reads pre-processing tools. Available from: http://hannonlabcshledu/fastx_toolkit/2010.
23. Kim D, Paggi JM, Park C, Bennett C, Salzberg SL. Graph-based genome alignment and genotyping with HISAT2 and HISAT-genotype. *Nat Biotechnol* 2019;**37**:907−15.
24. Liao Y, Smyth GK, Shi W. featureCounts: an efficient general purpose program for assigning sequence reads to genomic features. *Bioinformatics* 2014;**30**:923−30.
25. Love MI, Huber W, Anders S. Moderated estimation of fold change and dispersion for RNA-seq data with DESeq2. *Genome Biol* 2014;**15**:550.
26. Chen T, Liu Y, Huang L. ImageGP: an easy-to-use data visualization web server for scientific researchers. *iMeta* 2022:e5.
27. Subramanian A, Tamayo P, Mootha VK, Mukherjee S, Ebert BL, Gillette MA, et al. Gene set enrichment analysis: a knowledge-based approach for interpreting genome-wide expression profiles. *Proc Natl Acad Sci U S A* 2005;**102**:15545−50.
28. Zhou Y, Zhou B, Pache L, Chang M, Khodabakhshi AH, Tanaseichuk O, et al. Metascape provides a biologist-oriented resource for the analysis of systems-level datasets. *Nat Commun* 2019;**10**:1523.
29. Core Team R. R: a language and environment for statistical computing. Vienna, Austria: R Foundation for Statistical Computing; 2019. Available from: https://www.R-project.org/.
30. Jung MK, Mun JY. Sample preparation and imaging of exosomes by transmission electron microscopy. *J Vis Exp* 2018;**4**:56482.
31. Webber J, Clayton A. How pure are your vesicles?. *J Extracell Vesicles* 2013;**2**.
32. Zhuang X, Deng ZB, Mu J, Zhang L, Yan J, Miller D, et al. Ginger-derived nanoparticles protect against alcohol-induced liver damage. *J Extracell Vesicles* 2015;**4**:28713.
33. McGill MR. The past and present of serum aminotransferases and the future of liver injury biomarkers. *EXCLI J* 2016;**15**:817−28.
34. Im YR, Hunter H, de Gracia Hahn D, Duret A, Cheah Q, Dong J, et al. A systematic review of animal models of nafld finds high-fat, high-fructose diets most closely resemble human NAFLD. *Hepatology* 2021;**74**:1884−901.
35. Magee N, Ahamed F, Eppler N, Jones E, Ghosh P, He L, et al. Hepatic transcriptome profiling reveals early signatures associated with disease transition from non-alcoholic steatosis to steatohepatitis. *Liver Res* 2022;**6**:238−50.
36. Farrell G, Schattenberg JM, Leclercq I, Yeh MM, Goldin R, Teoh N, et al. Mouse models of nonalcoholic steatohepatitis: toward optimization of their relevance to human nonalcoholic steatohepatitis. *Hepatology* 2019;**69**:2241−57.
37. Cazanave S, Podtelezhnikov A, Jensen K, Seneshaw M, Kumar DP, Min HK, et al. The transcriptomic signature of disease development and progression of nonalcoholic fatty liver disease. *Sci Rep* 2017;**7**:17193.
38. Kim JK, Lee KS, Chang HY, Lee WK, Lee JI. Progression of diet induced nonalcoholic steatohepatitis is accompanied by increased expression of Kruppel-like-factor 10 in mice. *J Transl Med* 2014;**12**:186.
39. Sheth SS, Bodnar JS, Ghazalpour A, Thipphavong CK, Tsutsumi S, Tward AD, et al. Hepatocellular carcinoma in Txnip-deficient mice. *Oncogene* 2006;**25**:3528−36.
40. Lamkanfi M, Dixit VM. Inflammasomes and their roles in health and disease. *Annu Rev Cell Dev Biol* 2012;**28**:137−61.
41. Wu X, Dong L, Lin X, Li J. Relevance of the NLRP3 inflammasome in the pathogenesis of chronic liver disease. *Front Immunol* 2017;**8**:1728.
42. He Y, Zeng MY, Yang D, Motro B, Nunez G. NEK7 is an essential mediator of NLRP3 activation downstream of potassium efflux. *Nature* 2016;**530**:354−7.
43. McKnight AJ, Macfarlane AJ, Dri P, Turley L, Willis AC, Gordon S. Molecular cloning of F4/80, a murine macrophage-restricted cell surface glycoprotein with homology to the G-protein-linked transmembrane 7 hormone receptor family. *J Biol Chem* 1996;**271**:486−9.
44. Kisseleva T, Brenner D. Molecular and cellular mechanisms of liver fibrosis and its regression. *Nat Rev Gastroenterol Hepatol* 2021;**18**:151−66.
45. Carpino G, Morini S, Ginanni Corradini S, Franchitto A, Merli M, Siciliano M, et al. Alpha-SMA expression in hepatic stellate cells and quantitative analysis of hepatic fibrosis in cirrhosis and in recurrent chronic hepatitis after liver transplantation. *Dig Liver Dis* 2005;**37**:349−56.
46. Guido M, Rugge M, Leandro G, Fiel IM, Thung SN. Hepatic stellate cell immunodetection and cirrhotic evolution of viral hepatitis in liver allografts. *Hepatology* 1997;**26**:310−4.
47. Llovet JM, Kelley RK, Villanueva A, Singal AG, Pikarsky E, Roayaie S, et al. Hepatocellular carcinoma. *Nat Rev Dis Prim* 2021;**7**:6.
48. Luedde T, Kaplowitz N, Schwabe RF. Cell death and cell death responses in liver disease: mechanisms and clinical relevance. *Gastroenterology* 2014;**147**:765−783 e4.
49. Driedonks T, Jiang L, Carlson B, Han Z, Liu G, Queen SE, et al. Pharmacokinetics and biodistribution of extracellular vesicles administered intravenously and intranasally to *Macaca nemestrina*. *J Extracell Biol* 2022;**1**.
50. Gupta D, Liang X, Pavlova S, Wiklander OPB, Corso G, Zhao Y, et al. Quantification of extracellular vesicles *in vitro* and *in vivo* using sensitive bioluminescence imaging. *J Extracell Vesicles* 2020;**9**:1800222.
51. Cao M, Yan H, Han X, Weng L, Wei Q, Sun X, et al. Ginseng-derived nanoparticles alter macrophage polarization to inhibit melanoma growth. *J Immunother Cancer* 2019;**7**:326.
52. Mechta-Grigoriou F, Gerald D, Yaniv M. The mammalian Jun proteins: redundancy and specificity. *Oncogene* 2001;**20**:2378−89.
53. Meng Q, Xia Y. c-Jun, at the crossroad of the signaling network. *Protein Cell* 2011;**2**:889−98.
54. Liu T, Zhang L, Joo D, Sun SC. NF-κB signaling in inflammation. *Signal Transduct Targeted Ther* 2017;**2**:17023.
55. Hannemann N, Jordan J, Paul S, Reid S, Baenkler HW, Sonnewald S, et al. The AP-1 transcription factor c-Jun promotes arthritis by regulating cyclooxygenase-2 and arginase-1 expression in macrophages. *J Immunol* 2017;**198**:3605−14.
56. Jang S, Kelley KW, Johnson RW. Luteolin reduces IL-6 production in microglia by inhibiting JNK phosphorylation and activation of AP-1. *Proc Natl Acad Sci U S A* 2008;**105**:7534−9.
57. Francque SM, Bedossa P, Ratziu V, Anstee QM, Bugianesi E, Sanyal AJ, et al. A randomized, controlled trial of the Pan-PPAR agonist lanifibranor in NASH. *N Engl J Med* 2021;**385**:1547−58.
58. Dufour JF, Anstee QM, Bugianesi E, Harrison S, Loomba R, Paradis V, et al. Current therapies and new developments in NASH. *Gut* 2022;**71**:2123−34.
59. Younossi ZM, Ratziu V, Loomba R, Rinella M, Anstee QM, Goodman Z, et al. Obeticholic acid for the treatment of non-alcoholic steatohepatitis: interim analysis from a multicentre, randomised, placebo-controlled phase 3 trial. *Lancet* 2019;**394**:2184−96.
60. Al-Malki AL, Sayed AA. Bees' honey attenuation of metanil-yellow-induced hepatotoxicity in rats. *Evid Based Complement Alternat Med* 2013;**2013**:614580.
61. Korkmaz A, Kolankaya D. Anzer honey prevents *N*-ethylmaleimide-induced liver damage in rats. *Exp Toxicol Pathol* 2009;**61**:333−7.
62. Xiao J, Liu Y, Xing F, Leung TM, Liong EC, Tipoe GL. Bee's honey attenuates non-alcoholic steatohepatitis-induced hepatic injury through the regulation of thioredoxin-interacting protein-NLRP3 inflammasome pathway. *Eur J Nutr* 2016;**55**:1465−77.
63. Zhang S, Wu X, Bian S, Zhang Q, Liu L, Meng G, et al. Association between consumption frequency of honey and non-alcoholic fatty liver disease: results from a cross-sectional analysis based on the Tianjin Chronic Low-grade Systemic Inflammation and Health (TCLSIH) Cohort Study. *Br J Nutr* 2021;**125**:712−20.
64. Bahrami M, Ataie-Jafari A, Hosseini S, Foruzanfar MH, Rahmani M, Pajouhi M. Effects of natural honey consumption in diabetic patients: an 8-week randomized clinical trial. *Int J Food Sci Nutr* 2009;**60**:618−26.

65. Sadeghi F, Salehi S, Kohanmoo A, Akhlaghi M. Effect of natural honey on glycemic control and anthropometric measures of patients with type 2 diabetes: a randomized controlled crossover trial. *Int J Prev Med* 2019;**10**:3.
66. Cianciosi D, Forbes-Hernandez TY, Afrin S, Gasparrini M, Reboredo-Rodriguez P, Manna PP, et al. Phenolic compounds in honey and their associated health benefits: a review. *Molecules* 2018;**23**.
67. Dorn C, Engelmann JC, Saugspier M, Koch A, Hartmann A, Muller M, et al. Increased expression of c-Jun in nonalcoholic fatty liver disease. *Lab Invest* 2014;**94**:394−408.
68. Dela Pena A, Leclercq I, Field J, George J, Jones B, Farrell G. NF-kappaB activation, rather than TNF, mediates hepatic inflammation in a murine dietary model of steatohepatitis. *Gastroenterology* 2005;**129**:1663−74.
69. Schattenberg JM, Singh R, Wang Y, Lefkowitch JH, Rigoli RM, Scherer PE, et al. JNK1 but not JNK2 promotes the development of steatohepatitis in mice. *Hepatology* 2006;**43**:163−72.
70. Videla LA, Tapia G, Rodrigo R, Pettinelli P, Haim D, Santibanez C, et al. Liver NF-κB and AP-1 DNA binding in obese patients. *Obesity* 2009;**17**:973−9.
71. Ribeiro PS, Cortez-Pinto H, Sola S, Castro RE, Ramalho RM, Baptista A, et al. Hepatocyte apoptosis, expression of death receptors, and activation of NF-κB in the liver of nonalcoholic and alcoholic steatohepatitis patients. *Am J Gastroenterol* 2004;**99**:1708−17.
72. Kluwe J, Pradere JP, Gwak GY, Mencin A, De Minicis S, Osterreicher CH, et al. Modulation of hepatic fibrosis by c-Jun-N-terminal kinase inhibition. *Gastroenterology* 2010;**138**:347−59.
73. Beg AA, Sha WC, Bronson RT, Ghosh S, Baltimore D. Embryonic lethality and liver degeneration in mice lacking the RelA component of NF-κB. *Nature* 1995;**376**:167−70.
74. Eferl R, Sibilia M, Hilberg F, Fuchsbichler A, Kufferath I, Guertl B, et al. Functions of c-Jun in liver and heart development. *J Cell Biol* 1999;**145**:1049−61.
75. Sunami Y, Leithauser F, Gul S, Fiedler K, Guldiken N, Espenlaub S, et al. Hepatic activation of IKK/NFκB signaling induces liver fibrosis *via* macrophage-mediated chronic inflammation. *Hepatology* 2012;**56**:1117−28.
76. Csak T, Ganz M, Pespisa J, Kodys K, Dolganiuc A, Szabo G. Fatty acid and endotoxin activate inflammasomes in mouse hepatocytes that release danger signals to stimulate immune cells. *Hepatology* 2011;**54**:133−44.
77. Wree A, McGeough MD, Pena CA, Schlattjan M, Li H, Inzaugarat ME, et al. NLRP3 inflammasome activation is required for fibrosis development in NAFLD. *J Mol Med (Berl)* 2014;**92**:1069−82.
78. Mridha AR, Wree A, Robertson AAB, Yeh MM, Johnson CD, Van Rooyen DM, et al. NLRP3 inflammasome blockade reduces liver inflammation and fibrosis in experimental NASH in mice. *J Hepatol* 2017;**66**:1037−46.
79. Dixon LJ, Berk M, Thapaliya S, Papouchado BG, Feldstein AE. Caspase-1-mediated regulation of fibrogenesis in diet-induced steatohepatitis. *Lab Invest* 2012;**92**:713−23.
80. Dixon LJ, Flask CA, Papouchado BG, Feldstein AE, Nagy LE. Caspase-1 as a central regulator of high fat diet-induced non-alcoholic steatohepatitis. *PLoS One* 2013;**8**:e56100.
81. Schuster-Gaul S, Geisler LJ, McGeough MD, Johnson CD, Zagorska A, Li L, et al. ASK1 inhibition reduces cell death and hepatic fibrosis in an Nlrp3 mutant liver injury model. *JCI Insight* 2020;**5**:123294.
82. Gallego P, Castejon-Vega B, Del Campo JA, Cordero MD. The absence of NLRP3-inflammasome modulates hepatic fibrosis progression, lipid metabolism, and inflammation in KO NLRP3 mice during aging. *Cells* 2020;**9**:2148.